5-2013

Longitudinally Graded Optical Fibers

Alexander Evert
Clemson University, alex.g.evert@gmail.com

Longitudinally Graded Optical Fibers

A Thesis
Presented to
the Graduate School of
Clemson University

In Partial Fulfillment
of the Requirements for the Degree
Master of Science
Materials Science and Engineering

---

by
Alexander George Evert
May 2013

Accepted by:
Dr. John Ballato, Committee Chair
Dr. Phil Brown
Dr. Liang Dong

Abstract

Described herein, for the first time to the best of our knowledge, are optical fibers possessing significant compositional gradations along their length due to longitudinal control of the core glass composition. More specifically, MCVD-derived germanosilicate fibers were fabricated that exhibited a gradient of up to about 0.55 weight percent GeO_2 per meter. These gradients are about 1900 times greater than previously reported for fibers possessing longitudinal changes in composition. The refractive index difference is shown to change by about 0.001, representing a numerical aperture change of about 10 %, over a fiber length of less than 20 m. The lowest attenuation measured from the present longitudinally-graded fiber (LGF) was 82 dB/km at a wavelength of 1550 nm, though this is shown to result from extrinsic process-induced factors and could be reduced with further optimization. The stimulated Brillouin scattering (SBS) spectrum from the LGF exhibited a 4.4 dB increase in the spectral width, and thus reduction in Brillouin gain, relative to a standard commercial single mode fiber, over a fiber length of only 17 m.

Fibers with longitudinally uniform (i.e., not gradient) refractive index profiles but differing chemical compositions among various core layers were also fabricated to determine acoustic effects of the core slug method. The refractive index of the resulting preform varies by about $\pm$ 0.00013 from the average. Upon core drilling, it was found that the core slugs had been drilled off-center from the parent preform,

resulting in semi-circular core cross sections that were unable to guide light. As a result, optical analysis could not be conducted. Chemical composition data was obtained, however, and is described herein.

A third fiber produced was actively doped with ytterbium (Yb^{3+}) and fabricated similarly to the previous fibers. The preforms were doped via the solution doping method with a solution of 0.015 M Yb^{3+} derived from ytterbium chloride hexahydrate and 0.30 M Al^{3+} derived from aluminum chloride hexahydrate. The doped preform was engineered to have two core layers of differing chemical composition, resulting in both a gradient refractive index profile as well as a gradient acoustic profile. While exhibiting higher loss than the original LGF, the Yb^{3+}-doped fiber showed slightly better SBS suppression with preliminary calculations showing at least 6 dB reduction in Brillouin gain.

Lastly, reported here is a straight-forward and flexible method to fabricate silica optical fibers of circular cladding cross-section and rectilinear cores whose aspect ratio and refractive index profile changes with position along the fiber in a deterministic way. Specifically, a modification to the process developed to produce longitudinally-graded optical fibers, was employed. Herein reported are MCVD-derived germanosilicate fibers with rectangular cores where the aspect ratio changes by nearly 200 % and the average refractive index changed by about 5 %. Fiber losses were measured to be about 50 dB/km. Such rectangular core fibers are useful for a variety of telecommunication and biomedical applications and the dimensional and optical chirp provides a deterministic way to control further the modal properties of the fiber. Possible applications of longitudinally graded optical fibers and future improvements are also discussed.

The methods employed are very straight-forward and technically simple, providing for a wide variety of longitudinal refractive index and acoustic velocity profiles,

as well as core shapes, that could be especially valuable for SBS suppression in high energy laser systems. Next generation analogs, with longitudinally-graded compositional profiles that are very reasonable to fabricate, are shown computationally to be more effective at suppressing SBS than present alternatives, such as externally-applied temperature or strain gradients.

Dedication

To my friends and family. You have all helped in in more ways than you know and more than I'll ever be able to repay. Thank you all for being you.

Acknowledgments

First, I would like to thank Dr. John Ballato for giving me the opportunity to work in his group at the Center for Optical Materials Science and Engineering Technologies (COMSET) at Clemson University.

I would also like to acknowledge the invaluable assistance of the staff at COMSET and the Advanced Materials Research Laboratory, namely Andrew James–who first hired me as an undergraduate research assistant–and Dale Edmonson for their help in fabricating my preforms and teaching me how to use the MCVD lathe. Dr. Paul Foy, Wade Hawkins, Devon McClane, Max Jones, and Chris Dunn for their work on the draw tower, drawing my (very complex) preforms into fiber, and Donald Mulwee in Clemson's electron microscopy lab who assisted with imaging and chemical composition analysis of my fiber.

Thank you to Jeff Page of AFL Telecommunications in Spartanburg, South Carolina for early assistance on OTDR, Dr. Larry McCandlish of Ceramare as well as Kirk Schoell of Cidra Precision Services, LLC for their help in machining our glass, Dr. Pete Dragic at the University of Illinois at Urbana-Champaign for conducting SBS measurements and Dr. Andrew Yablon at Interfiber Analysis for their help in analyzing the optical properties my fiber.

Table of Contents

List of Tables

List of Figures

Chapter 1

Introduction

Light has been used as a medium for communication for as long as civilization has existed. From the smoke signals of pre-history to semaphore flags used for ship-to-ship communication, most of these methods have been crude, range limited, unable to carry much information at any given time, and dependent upon line-of-sight.

Two limiting factors have historically prevented the widespread use of optically based communications networks. The first being the lack of a loss material and the second being the lack of a light source powerful enough for the long distances involved. Low loss optical fiber became feasible after a new method of producing glass—the first in several millennia— was developed by Corning Incorporated in which liquid chemicals were reacted with oxygen in the presence of heat to form glass [4]. After the invention of the laser in the 1960s as a practical light source, the development of optical fiber communications systems became feasible. Subsequent improvements in both technologies over the ensuing years allowed for the vast network of fiber that forms the backbone of the internet, cellular phones, and myriad other modern communications methods to come to fruition.

While optical fiber has many advantages over other communication methods,

including increased bandwidth capability, and low loss and cost per meter when compared to copper [5], it also has some disadvantages. Optically, if silica is contaminated with water during processing, a strong hydroxyl absorption peak, as shown in figure 1.1. As a result, any water contamination can be extremely poisonous to the propagating signal (water levels with today's fabrication techniques are down to the parts per billion level or lower [6]). Other notable impurities include transition metals in various valence states. (Fe^{2+} gives the green-blue color found in older or decorative glass) [7]. Therefore, the purity of the glass and precursor chemicals during manufacture must be kept very high, adding to capital costs. Standard optical fibers are also limited by the amount of input power they can accept. Higher input power levels can result in such deleterious effects such as four-wave mixing (FWM), the combination of multiple wavelength channels interfering, producing new waves at the sum and difference beat frequencies, thereby robbing the initial signal of power. Finally, whereas copper wire can merely be welded to subsequent sections when extra length is needed, silica fibers must be perfectly lined up when fused to prevent core misalignment that would otherwise result in the signal being unable to propagate. This necessitates the use of expensive high-precision equipment and more time-consuming installation procedures.

An issue with fiber utilization that is related more to its application rather than production is that of fiber-to-the-home (FTTH) installations for internet networks. Until recently, it has been economically unfeasible for telecommunications companies to lay fiber lines to individual households. Indeed, for most United States citizens not living in large cities, FTTH is still economically untenable due to our relatively low national population density. Instead, the copper coaxial cables that have been used for cable television for decades are used to transmit data from households to local or neighborhood nodes where the signal is then transferred to optical fiber.

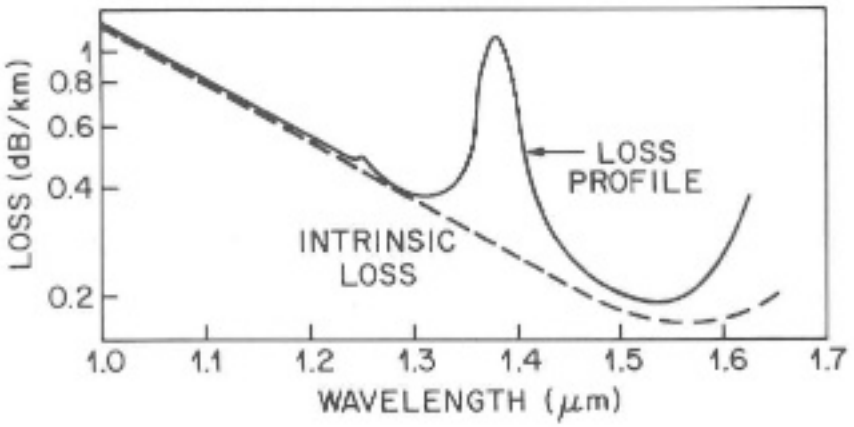

Figure 1.1: Loss in silica optical fiber. The dashed line represents the loss intrinsic to silica. The solid line shows hydroxyl absorption peaks at $\sim 1.37\mu$m and $\sim 1.23\mu$m. From [1]

However, with more households subscribing to high-speed internet services and the higher bandwidth requirements associated therewith (and hence, higher subscription costs for providers), FTTH becomes more economically palatable [8].

Despite the drawbacks, optical fiber has proliferated throughout the world. The vast majority of fiber is silica based, with a core doped with several weight percent germania which serves to increase the refractive index of the fiber core. The core is surrounded by a lower index cladding, usually pure silica but sometimes doped with chemicals that depress refractive index, such as fluorine. Refractive behavior is governed by Snell's Law, which states that the angle of refraction, θ_t, is proportional to the sine of the angle of incidence, θ_i. Put mathematically, Snell's Law is

$$n_i sin(\theta_i) = n_t sin(\theta_t) \tag{1.1}$$

where n_i and n_t are the refractive indecies of the core and cladding, respectively. The increased refractive index in the core allows light to be guided through

the fiber through a phenomenon called total internal reflection (TIR) as opposed to being scattered. TIR occurs only when the input light strikes the surface of the fiber within a given cone. The minimum angle from face of the fiber in which the light will refract and guide through the fiber is known as the critical angle, θ_c. The critical angle is the angle at which incident light will transmit along the surface of the fiber. At this angle of incidence, θ_t will be 90°. Rearranging equation (1.1) and plugging in 90° for θ_t gives

$$sin(\theta_c)(n_i/n_t) = sin(90) = 1 \tag{1.2}$$

$$\theta_c = arcsin(n_t/n_i) \tag{1.3}$$

θ_c is dependent upon the numerical aperture of the fiber (which in turn is dependent on the difference in refractive index between core and cladding) and is given by

$$NA = (n_1^2 - n_2^2)^{1/2} \tag{1.4}$$

While the majority of optical fiber is fabricated to have a consistent refractive index profile along its length, methods have been devised to modify the refractive index of an optical fiber at points along its length either permanently (e.g., by modifying fiber diameter during the draw or by tapering [9]) or transiently (e.g., using temperature [10] or strain [11]). Such perturbations influence the modal or propagation characteristics of the optical (or acoustic) field in the fiber and, consequently, have been used to control nonlinearities [12], including chromatic dispersion and soliton propagation [9], and suppress stimulated Brillouin scattering (SBS) [13] and four-

wave mixing (FWM) [14], to name just a few applications. For completeness, it is worth noting that the benefits to suppressing Brillouin oscillations in fibers using compositional gradients had been conjectured over 30 years ago [15].

Fibers possessing longitudinal changes in composition previously have been realized [16], [17] using vapor-axial deposition (VAD). However, since the composition was changed along the length of the entire preform, the resultant longitudinal compositional gradient in the drawn fiber was very low, just 0.4% over 28 km of length. While such a length is acceptable for long-haul telecommunication applications, many other applications for optical fibers exist, such as high energy lasers, where shorter lengths of fibers possessing higher longitudinal gradients are of interest.

In this thesis, a straight-forward method is developed in order to controllably shape the compositional profile of the core along a short length of optical fiber, presently on the order of 100 m, but conceivably a meter or less depending on the gradient. By controlling the properties of the fiber along its length through the core glass composition, rather than dimension, strain, or temperature, a new family of property-enhanced optical fibers are realized.

1.1 Non-linear Optical Effects (NLOEs)

Most everyday interactions of light with optical systems can be described by the classical electromagnetic theory. Transmittance and reflectance (as observed in windows and mirrors, respectively) and refraction (prisms, corrective lenses, the bent straw in a glass of water) can be described by equations that depend only on the wavelength of light and its velocity in a given medium [18]. Both reflection and refraction can be described with simple geometry. The law of reflection states that reflected light will remain in the plane of the incident light, and the angle of reflection,

θ_r, is equal to the angle of incidence, θ_i. The law of refraction, as described previously, governs the transmittance of light through two media of differing refractive indecies.

As with reflection, refracted light stays within the same plane as the incident light [18]. However, higher power and more coherent light sources, such as those found in lasers, can cause the optical properties of the material through which the light is propagating to become a function of the light's electric field intensity. These nonlinear effects, as they are known, arise due to the inability of electric dipoles in the optical medium to respond linearly to the light alternating electric field ($\overrightarrow{E}$-field). Valence band electrons drive electric polarization as the atomic nulei and inner-core electrons are too massive and tightly bound, respectively, to respond to the alternating $\overrightarrow{E}$-field of visible light (roughly 10^{14} - 10^{15} Hz). Specifically, silica is transparent in the visible spectrum but absorbs ultraviolet light due to electronic transitions and infrared light due to vibrational (multi-phonon) absorption [19].

When a given materially-dependent threshold of intensity is reached, the linear proportionality of polarization to the electric field begins to fail and nonlinear effects become noticeable. In such a case when two or more light waves interfere, the principle of superposition no longer holds, meaning the net displacement is no longer equal to the sum of the displacements of the individual waves, and nonlinear equations must be utilized to describe the light's behavior [18]. In order to properly describe nonlinear behavior, classical (linear) electromagnetic theory must be extended to accommodate the observed responses.

The polarization, $\overrightarrow{P}$, of a medium due to the presence of an electric field is generally written as

$$\overrightarrow{P} = \epsilon_0 \cdot \chi \cdot \overrightarrow{E} \tag{1.5}$$

where χ is the susceptibility and ϵ_0 is the permittivity of vacuum ($\epsilon_0 = 8.854 \cdot 10^{-12}$ C^2/N$\cdot$m^2). The nonlinear susceptibility dominates considerations in nonlinear optics and constitutes the material response to an applied electromagnetic field. When the variations from linearity are small, the susceptibility in nonlinear media can be modeled as

$$\chi = \chi_1 + \chi_2 E + \chi_3 E^2 + \cdots + \chi_n E^{n-1} \tag{1.6}$$

which, when substituted into 1.5 yields

$$P = \epsilon_0(\chi_1 E + \chi_2 E^2 + \chi_3 E^3 + \cdots + \chi_n E^n) \tag{1.7}$$

It should be noted that Equation 1.7 describes polarization *strength*. In linear optics, the χ_1E term dominates. It is third order effects ($\chi_3 E^3$) in which stimulated Brillouin scattering and other effects described herein occur [18].

Second order nonlinear effects result from polarization being proportional to the square of the electric field. Because there is little to no contribution of second order effects in isotropic materials or materials containing a crystallographic center of symmetry (center of inversion), they are not found in standard optical fiber [18]. Nonetheless, there are several second order NLOEs, such as parametric amplification and frequency mixing [20].

Numerous third order non-linear optical effects (NLOEs) are associated with silica-based optical fiber, including the aforementioned FWM, and SBS (to be discussed in detail later). Other effects include Stimulated Raman Scattering (SRS), Self- and Cross-Phase Modulation (SPM and XPM, respectively), soliton formation, and modulation instability (MI) [21], [22]. Stimulated Raman scattering is similar to SBS, but occurs at higher input light power levels and results in much larger frequency

downshifts in the scattered light (on the order of 10 THz at 1550 nm) as well as a wider bandwidth. Self-phase modulation occurs when high level coupled output light modulates its own phase and either broadens or compresses (depending on the sign of the chromatic dispersion) the transmitted signal. Thus, the leading edge of the signal shifts to long wavelengths and the trailing edge shifts to shorter wavelengths. Cross-phase modulation broadens the signal spectrum when optical intensity changes due to interactions between adjacent channels, resulting in interference between channels. XPM can be minimized by ensuring enough physical spacing between channels. Modulation instability breaks continuous wave signals into a modulated structure. MI can be viewed as a particular case of FWM where two incident photons are converted into two photons of different frequencies. Finally, solitons are pulses that do not change shape (broadening due to dispersive effects), as they traverse the fiber due to a balance between dispersion and nonlinearities. Solitons result in high signal degradation but can be avoided by operating below the zero-dispersion wavelength [23]. The lack of signal broadening is very desirable in optical fiber, as this means that consecutive signals can be sent in more rapid succession without fear that the signals will mix into a single undefined signal on the receiving end of the fiber.

All NLOEs can be classified into two general categories: scattering effects (e.g., SBS and SRS) and effects related to the Kerr Effect—the change of the refractive index of a material as a function of the intensity of an electric field [21]. The Kerr effect gives rise to several of the secondary effects mentioned previously, such as self-phase modulation, cross-phase modulation, four wave mixing, and modulation instability [12]. The change in reactive index arising from Kerr effects can be expressed by

$$n(I) = n_0 + n_2 I \tag{1.8}$$

where n_0 is the linear refractive index and n_2 includes the nonlinear effects induced by polarization. Because intensity (I) is proportional to the square of the electric field (i.e., $I = E^2(\omega)/2$), The Kerr Effect has a quadratic dependence with the electric field [20]. The Kerr effect can be advantageously exploited for optical parametric-amplification frequency conversion [24], optical phase conjugation [25], and pulse compression and regeneration [26].

Non-linear optical effects begin appearing at higher signal powers and/or longer transmission distances. But unless efforts are made during fabrication to achieve phase matching, processes resulting in the generation of new frequencies are not efficient in optical fiber. Thus, the most important NLOEs in optical fiber arise from nonlinear refraction [1]. When one considers that long distance fiber optic communication systems must cover hundreds of miles with as few amplifiers as possible in order to minimize cost, the temptation is to compensate by increasing input power. However, as noted, with higher input power comes a greater likelihood of encountering NLOEs, thus potentially negating any added benefit of increasing input power levels. The lowest power threshold effect, stimulated Brillouin scattering, the causes of SBS, and a novel method of SBS suppression will be the leading subject of this thesis.

1.2 SBS Causes, Effects, and Suppression

Brillouin scattering is named after Leon Brillouin, the French physicist who predicted its existence in 1922 [27], although stimulated Brillouin scattering was not observed until 1964 [28]. Simply, Brillouin scattering results from incident light scattering by acoustic waves. In spontaneous Brillouin scattering, an incident light wave (the signal being propagated down the fiber) is transformed into a phonon and a

scattered light wave (Stokes wave) via Bragg diffraction due to slight changes in refractive index caused by minute temperature differences along the length of the fiber [2]. Spontaneous Brillouin scattering is weak and usually ignored. The process is considered to be spontaneous because the scattering takes place under conditions such that the optical properties of the material are unaffected by the incident electric field of the light. SBS is of interest because it has the lowest threshold power of the previously described NLOEs. For a 10 km fiber the SBS threshold can be around 10 mW when a continuous wave laser is used as the light source [29].

Stimulated Brillouin scattering is caused by electrostriction, a phenomenon by which dielectrics (polarizable electric insulators) change their dimensions in the presence of an electric field [30]. In the case of optical fibers, electrostriction results from the electric field of the propagating light and generates a moving acoustic wave in the fiber. This acoustic wave creates a moving variation in the density of the glass along the fiber length, thereby periodically modulating the refractive index. This refractive index grating scatters light through Bragg diffraction, a phenomenon in which light of specific wavelengths is reflected while others continue propagating normally. Because the gratings are moving at the speed of sound for the material, the diffracted light is Doppler-shifted to a lower frequency and now propagating in the backward direction compared to the input light [2]. Typically, the Brillouin frequency shift is around 10 GHz for silica when the incident light is at a wavelength of about 1550 nm [31], a standard wavelength for commercial telecommunications. The backscattered light further interacts with subsequent input light, creating a beat, shown in figure 1.2, of moving acoustic waves and interference patterns.

The threshold for SBS generation (G) is defined by

$$G = gI_L(0)L \tag{1.9}$$

where g is the SBS gain factor, $I_L(0)$ is the the intensity of the incident laser light, and L is the length of the fiber (or other optical medium). For SBS to occur, G will typically be on the order of 25 [32].

The magnitude of frequency shift depends on the scattering angle, but given the small core area and long lengths of optical fiber, only the $\theta = 0°$ and $\theta = 180°$. At these angles, the shift is at a maximum and the frequency shift is given by the equation:

$$\nu_B = \frac{2nV_A}{\lambda_p} \tag{1.10}$$

where λ_p, n, and V_A are the pump wavelength, refractive index of the core, and sound velocity of the material, respectively [33]. The speed of sound through a material is dependent on the material's density, ρ, and modulus of elasticity, E_0, and can be determined by:

$$V_A = \sqrt{\frac{E_0}{\rho}} \tag{1.11}$$

The combination of the diffracted light and forward propagating acoustic wave means the original forward propagating input signal must be limited in its power. If the SBS threshold is reached, significant attenuation of the propagating signal will occur. This thesis will describe a new method of SBS reduction that is especially applicable over shorter distances (< 1 km).

The SBS threshold can generally be increased in two ways [13]:

1. Broadening the line width of the laser by phase or frequency modulation

2. Broadening the Brillouin-gain bandwidth by varying the frequency of the acoustic wave along the fiber.

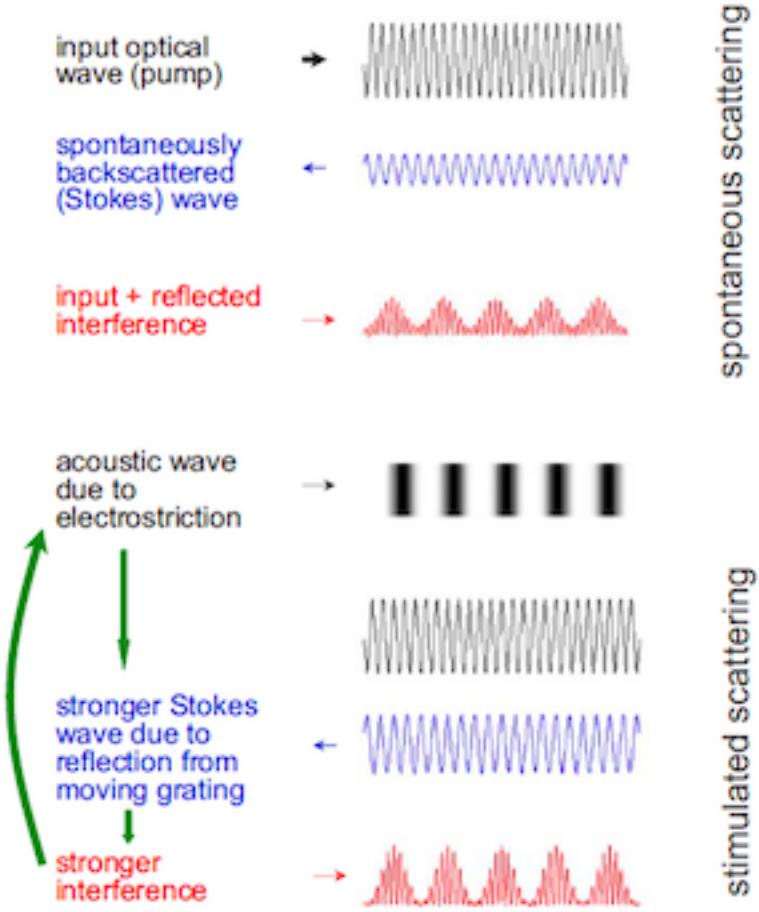

Figure 1.2: Depiction of the various acoustic and optical waves associated with spontaneous (top) and stimulated (bottom) Brillouin scattering. From [2].

Method number two can be implemented by varying the core radius, chemical composition, temperature, or by introducing a physical strain on the fiber, as previously cited.

Due to the long lengths and small cross sections of optical fiber, the forward Brillouin scattering is negligibly weak, so the Stokes wave propagates in the backward direction to the input wave. This backward propagating wave interferes with the oncoming signal wave, adding energy to the acoustic waves and increasing the likelihood of additional scattering through Bragg diffraction [2]. The frequencies and wave vectors of the pump and scattered light, as well as the acoustic fields are given by:

$$\Omega_B = \omega_p - \omega_S, \overrightarrow{q} = \overrightarrow{k_p} - \overrightarrow{k_S} \tag{1.12}$$

where $\omega_{p,S}$ and $k_{p,S}$ are the optical (angular) frequencies and wave vectors of the pump and Stokes fields, respectively. The Brillouin frequency, Ω_B, and wave vector of the acoustic field, q, are related by

$$\Omega_B = |\overrightarrow{q}| \cdot \nu_A \approx 2\nu_A \cdot |\overrightarrow{k_p}| \cdot sin(\theta/2) \tag{1.13}$$

where ν_A is the speed of sound in the medium and θ is the angle between the pump and Stokes fields [31]. Again, due to the geometry of optical fibers, i.e., small core diameters and long lengths, the scattered light propagates forward and backward, i.e., $\theta = 0$ and π.

The interaction of the forward and backward light waves results in amplification of the sound wave at the expense of the forward propagating optical wave. When the power of the input pump reaches a given threshold level, the process becomes stimulated, resulting in the process becoming strongly dependent on pump

power and the conversion from input to backscattered light becoming very efficient. The specific amount of energy to initiate SBS is dependent upon the material composition [16], [17], core radius [34] temperature [10], or strain induced on the fiber [35]. The threshold for SBS for a continuous wave light source can be approximated by [36], [37]:

$$P_{th} = 21\frac{KA_{eff}}{g_0 L_{eff}} \cdot \frac{\nu_B - \nu_L}{\Delta\nu_{Int}} \tag{1.14}$$

where K is the polarization factor, A_{eff} is the effective area of the fiber core, and ν_p and ν_B are the pump light line width and Brillouin bandwidth, respectively. g_0 is the the Brillouin gain coefficient, and L_{eff} is the effective fiber length as defined by:

$$L_{eff} = \frac{1 - e^{-\alpha L}}{\alpha} \tag{1.15}$$

where α is the fiber attenuation coefficient and L is the fiber length [36].

The SBS threshold (SBST) is generally defined by a fraction, μ, of the output (backscattered) Stokes power compared to the maximum signal power. The specific value of μ is not critical, however, due to the exponential dependence of Stokes power on input pump power. More important is the realization that Stokes power rapidly increases and approaches the input power so higher order Stokes waves can be generated [2].

SBS is not always considered to be a deleterious effect. Indeed, many applications take advantage of SBS for efficient narrowband amplification, provided the Stokes wave is seeded from the rear (non-input) end of the fiber. Brillouin fiber amplifiers (BFAs) have found use in microwave photonics systems [38], shape-adjustable narrowband optical fiber [39], millimeter wave signals [40], and tunable slow-light

delay buffers [41].

1.3 Non-circular Fiber Cores

There has been remarkable growth in the design of optical fibers as greater demands are placed on their performance. Single mode fibers for telecommunications gave way to dispersion-compensating fibers [42]. Conventional core size and numerical aperture designs for optical amplifiers gave way to large mode area designs for high energy lasers [43], [44]. Simple core/clad geometries continue to give way to microstructured and photonic bandgap configurations where the modal properties of the light as well as light/matter interactions such as SBS [45], [46] can be controlled to a great degree through fiber design. However, with complexity generally comes difficulty in manufacturability, hence yield and cost.

Recently, a versatile and straight-forward method was reported for the fabrication of optical fibers possessing longitudinally-graded compositions; hence longitudinally-graded optical and/or acoustic properties [47], [3]. Here, a variant of the longitudinally-graded optical fiber (LGF) fabrication process is employed in order to realize cores of rectilinear cross-section (i.e. rectilinear core fiber, or RCF), including those with a dimensional chirp of core width with constant fiber diameter. Conceptually, to create an LGF, a silica-based preform is fabricated using chemical vapor deposition methods (e.g., MCVD, OVD, VAD) and is referred-to here as the parent perform. A rod of glass is core-drilled out through the side of this parent preform. This rod, or slug, is then sleeved into a fluorosilicate cladding tube, consolidated, and drawn into fiber. If the radial refractive index profile (for example) of the mother preform is non-uniform, this is transformed into a longitudinal profile in this manner in the final fiber, creating the LGF. In order to create an RCF, the side-core-drill diameter

is larger than the core diameter of the original parent preform such that the resultant slug contains regions of the silica glass cladding around the core. When sleeved into the (fluorinated silica) cladding tube and viewed from the longitudinal perspective, this results in a rectangular core as is shown schematically in figure 2.1 [a-c]. In contrast to the fabrication of RCFs, optimal LGF gradients occur where the diameter of the side-core-drill is equal to or smaller than the core diameter of the parent perform, or even taken from a plane-stratified bulk material. This gives rise to greater homogeneity and maximizes the gradient across the whole final fiber core. In the case of an RCF a compositional gradient can be achieved (if an LGF parent preform is used) or the composition can be uniform (if a conventional preform is used). This versatility therein provides an extra tool in the toolbox of the fiber designer.

In the case where a refractive index (or other) gradient is desired, the parent perform will likely have a core that is radially-graded. Referring to figure 2.1, the wide rectilinear axis of the final core corresponds to the longitudinal axis in the parent perform, and therefore the refractive index distribution along (or parallel to) this axis would be uniform. However, the narrow rectilinear axis of the final fiber corresponds to a chord across the parent perform core, perpendicular to the core-drill axis, which is graded. Therefore, the narrow axis of the rectilinear core of an LGF will also be graded, but will be symmetric with its refractive index peaking in the center. Similarly, the outer edges of the narrow rectilinear axis will also have slightly lower longitudinal gradients than the central region. This results from the fact that the central region longitudinal gradient (of the final fiber) subtends the core diameter chord parallel to the core-drill axis, while those of the outer edges subtend smaller chords parallel to the core-drill axis. In the limit such a chord, decreasing in size approaching the edge of the fiber mother perform core, would have a diminishing longitudinal gradient. All of these issues are considerations in the design of an LGF

RGF.

Whether or not the core has an index or acoustic gradient, as permitted using the LGF process, such rectilinear core optical fibers have been modeled electromagnetically [48], [49] and could be useful for a variety of applications including polarization-maintaining fibers [50], self-filtering of signals in telecommunication [51], mode conversion [52], biomedical imaging [53], and single-mode ultra-large core area fibers for high energy lasers [54]. Such fibers also could potentially facilitate efficient coupling to broad stripe laser diodes. Fibers with non-circular cores have been fabricated previously using pressure-assisted approaches [55] and applying heating profiles around the preform causing it to deposit soot and collapse non-uniformly [56]. Non-circular fibers are also commercially-available [57]. However, the added value of this work lies in the realization of chirped non-circular fibers whose core dimension deterministically changes along the fibers length and, therefore, enhances design flexibility to core geometry.

Fibers with circular cores are by far the most commonly produced due to their ease of fabrication and isotropic cross-sectional areas. However, it is possible (and in some cases desirable) to fabricate fiber cores with non-circular cross sections. Cores with rectangular [58], [59], square [60], elliptical [61] and double elliptical [62], [63] cross sections have been produced. D-shaped fibers, which have a circular core but the cladding is cut to a flat face on one side to within a few microns of the core-clad interface so that an appreciable optical field exists outside the fiber, have also been produced [64]. Such irregularly shaped cores can help to overcome some issues with conventional single-mode fibers, specifically the tendency in circular core fibers to depolarize light in very short distances, usually just a few centimeters [63]. Additionally, circular core fibers are limited in their high power applications due to stimulated Raman scattering and thermal lensing [58].

Rectangular (and square) cores allow for more efficient transfer of heat away from the core by increasing cross-sectional area of the core/cladding interface along the fiber length. For an object of a given area, a circular cross section will give the shortest perimeter and, correspondingly, the smallest surface area of a 3D projection of that cross section. (By way of example, a circle with an area of π will have a perimeter of 2π or ~ 6.28, whereas a square with an area of π will have an perimeter of $4\sqrt{\pi}$ or ~ 7.09). This smaller surface area on a circular cylinder corresponds to lower surface energy and therefore a more stable shape. The high temperatures involved with drawing optical fiber allow the glass to more easily flow and therefore seek the more thermodynamically stable circular shape. Thus, the corners of square and rectangular core fibers will generally be rounded, the degree of which depends on the set point temperature, the time spent at said temperature, and the specific material used. Nonetheless, methods have been devised to preserve the desired shapes to a great extent. So called flat fibers have been developed using an MCVD technique that utilizes a square preform tube and omits collapse of the tube on the lathe. Instead, the preform is kept under vacuum during drawing, resulting in both a rectangular core and fiber [59]. Another method uses the more common cylindrical preform tubes but a high-temperature ceramic cylinder (such as zirconia) with various patterns cut into it shields parts of the tube as the burner traverses. The shielding results in uneven heating of the tube around its inner circumference, which in turn gives an uneven soot profile that results in non-circular core geometries [56]. Crystalline silicon square cores have also been made by melting silicon (crystalline) rods inside a square silica (glass) cladding tube. The lower melting point of crystalline silica allows the semiconducting metal to take the shape of the cladding tube while being drawn, although during cooling, the differing melting points and coefficients of thermal expansion can result in core/clad interface separation [65].

Square and rectangular cores are primarily useful in applications such as directional filters and couplers [66] as well as in laser etching applications, such as solar panel fabrication [67] where the Gaussian intensity distribution can result in over-penetration near the center (i.e., highest intensity) of the laser's path and cause damage to underlying layers not intended to be etched at a given point. This problem is mitigated with square core fiber lasers due to the more homogenous power distribution across the core area.

D-shaped fibers can be used in optical sensors, polarizers, fiber couplers, and tunable fiber components [68]. They are often used in hostile environments due to silica's extreme resistance to high temperature and chemical attack. This, combined with with fiber's high bandwidth (which results in higher resolution data), makes such sensors attractive over traditional electronic sensors [69]. Because part of the field is transmitted outside the fiber, the strength of the field is dependent on the environment. This characteristic can be useful in chemical sensors that detect the presence of chemicals, such as methane, by absorption of specific wavelengths [70].

Elliptical core fibers are highly birefringent (refractive index is dependent on polarization), which lends its use to sensors to measure physical parameters such a temperature, pressure, and elongation [71]. Elliptical core fibers can propagate two fundamental modes that correspond to the major and minor axes of the ellipse. Double elliptical core fibers have been investigated for use as photonics band gap fibers and surface plasmonic waveguides [64], [62]

Chapter 2

Fiber Design and Analysis

In this chapter, a straight-forward method is detailed that allows for controllably shaping the compositional profile of the glass core along a short length (presently about 10 - 20 m, but conceivably a meter or less depending on the gradient) of optical fiber. By controlling the properties of the fiber along its length through the core glass composition—rather than dimension, strain, or temperature—a series of other useful opportunities present themselves including longitudinally-graded rare-earth doped fibers or fibers that possess a uniform refractive index but gradient acoustic velocity. An appendix is provided following the conclusion of chapter 4 to discuss more subtle considerations such as the influence of longitudinal-gradients on numerical aperture and fiber attenuation.

A depiction of the general process developed is shown in figure 2.1 and follows the scheme described by Rice, et al. [47]. Conceptually, a radial refractive index profile is generated in a silica preform using conventional chemical vapor deposition methods [72]. This radial profile is transformed into a longitudinal profile by core-drilling a rod through the side of the preform. This rod, which contains a portion of the core as well as two end sections of the cladding glass (figure 2.1[b]), is then sleeved

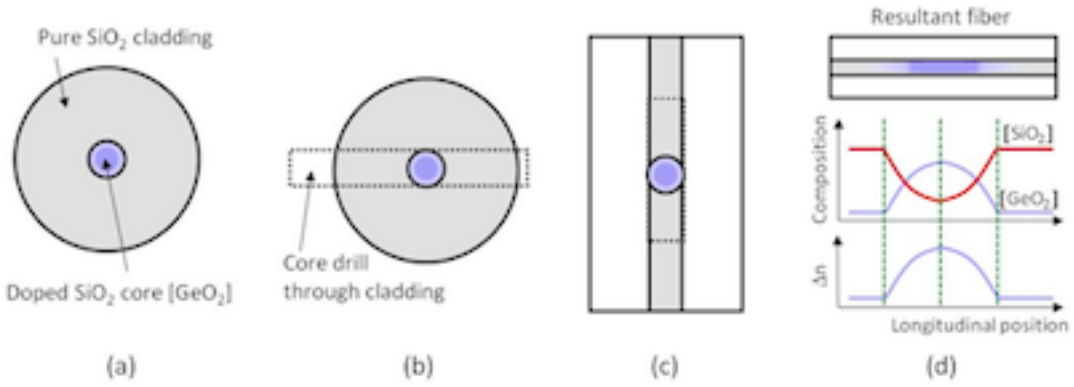

Figure 2.1: Idealized representation of the process employed. (a) Conventional GeO_2-doped SiO_2 preform fabricated with specific radial refractive index profile using a chemical vapor deposition process; (b) a rod is core-drilled out through the side of the preform such that radial gradient of the preform becomes a longitudinal gradient in the rod; (c) rod from (b) is sleeved into a lower refractive index inner cladding tube such that a index-guiding core/clad geometry is achieved; (d) preform from (c) is drawn into fiber such that longitudinal refractive index profile is now present in the optical fiber. Also shown in (d) are the idealized longitudinal refractive index and compositional profiles of the fiber; which are correlated and are defined by the initial radial profile of the preform in (a). The vertical green dotted lines in (d) are guides to the eye.

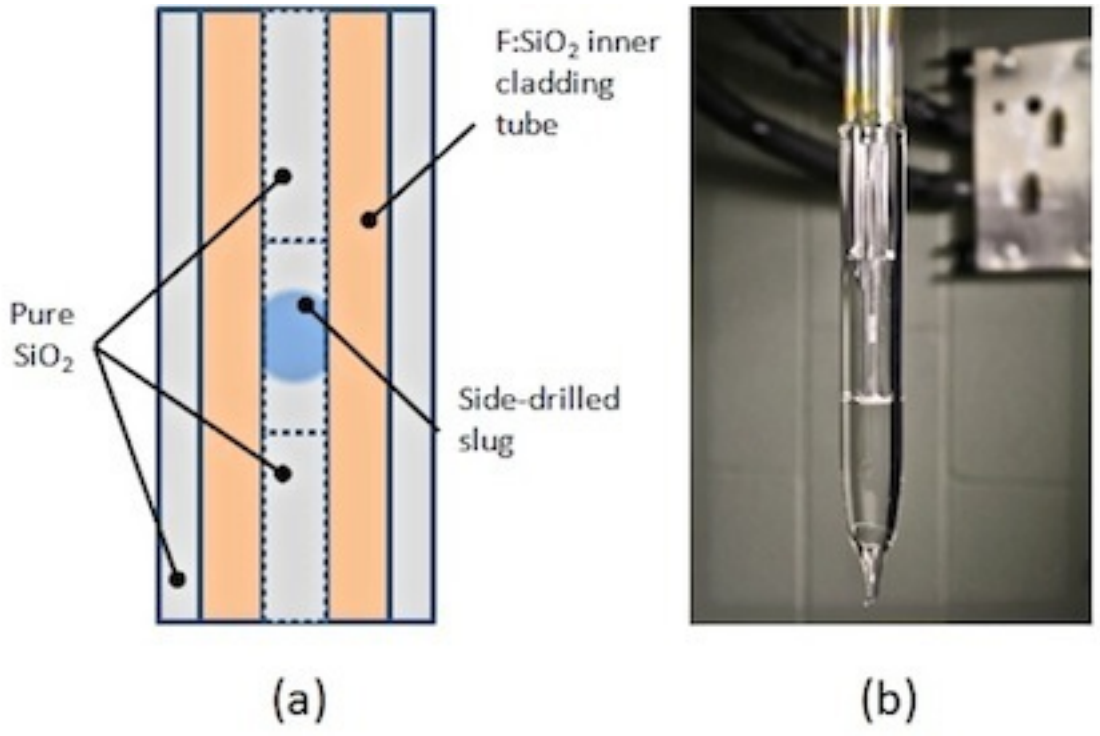

Figure 2.2: Illustration (a) showing the workup with the core pictured in the middle, sleeved inside fluorinated silica (orange, which is then sleeved inside pure silica (outer gray). The actual preform prior to draw is shown in (b). The core is plainly visible in the middle of the consolidated preform, the result of tool markings from the core drilling process.

inside a lower refractive index tube, now acting as the preform, for the subsequent drawing of the longitudinally-graded optical fiber (LGF). An illustration showing assembled preform as well as a photograph of the actual preform just prior to drawing are shown in figure 2.2.

More specifically, a doped SiO_2 preform was fabricated using an SG Controls modified chemical vapor deposition (MCVD) lathe (Clemson University). The preform was fabricated from a pure silica tube that was about 450 mm in length and had an inner and outer diameter of 17 and 21 mm, respectively. The core region consisted of four deposition layers. The first three were doped with germanium from a $GeCl_4$

vapor source. The $GeCl_4$ flow rate was increased by 2 standard cubic centimeters per minute (sccm) per layer from about 30 sccm for the first layer to about 34 sccm for the third layer. A constant flow of $SiCl_4$ at about 60 sccm was maintained throughout the first three layers. The fourth layer was co-doped with $GeCl_4$ at about 100 sccm and SiF_4 at about 70 sccm. The use of fluorine-doping in this last core layer was to investigate whether an additional dopant could measurably influence either the longitudinal optical or the acoustic properties of the resultant fiber. During the preform collapse stage, a low flow of SiF_4 was maintained in order to lessen fluorine losses. For completeness, note that the fluorine is too light of an element to be measured using the energy dispersive x-ray spectroscopy analytical methods described below. Accordingly, the fluorine is not discussed with respect to the chemistry of the core but could influence both the optical and acoustic behavior. However, since the fluorine level is fairly low, based on the SiF_4 flow rates, its impact on the performance of these proof-of-concept fibers is not expected to be large compared to that of the GeO_2 doping. The radial refractive index of the resulting preform was profiled using a Photon Kinetics PK2600 preform analyzer at 10 mm increments. The refractive index profile at the location of the core slug used for drawing is shown in figure 2.3. Scans started at a position of 50 mm and ended at 260 mm as measured from the preform tip. Rods comprising the 1.7 mm diameter core then were transversely-drilled through the full diameter of the preform (Ceramare, Piscataway, NJ; later cores drilled at Cidra Precision, Wallingford, CT) at the same locations as index profiled on the PK2600. Surface finish of the initial core slugs was subsequently marginally improved (Great Lakes Glasswerks, Painesville, OH) however the surface quality was still relatively poor upon drawing. Later core slugs showed yet better surface finish without subsequent attempts at polishing.

One of the side-core-drilled slugs (figure 2.4) was sleeved into a fluorinated

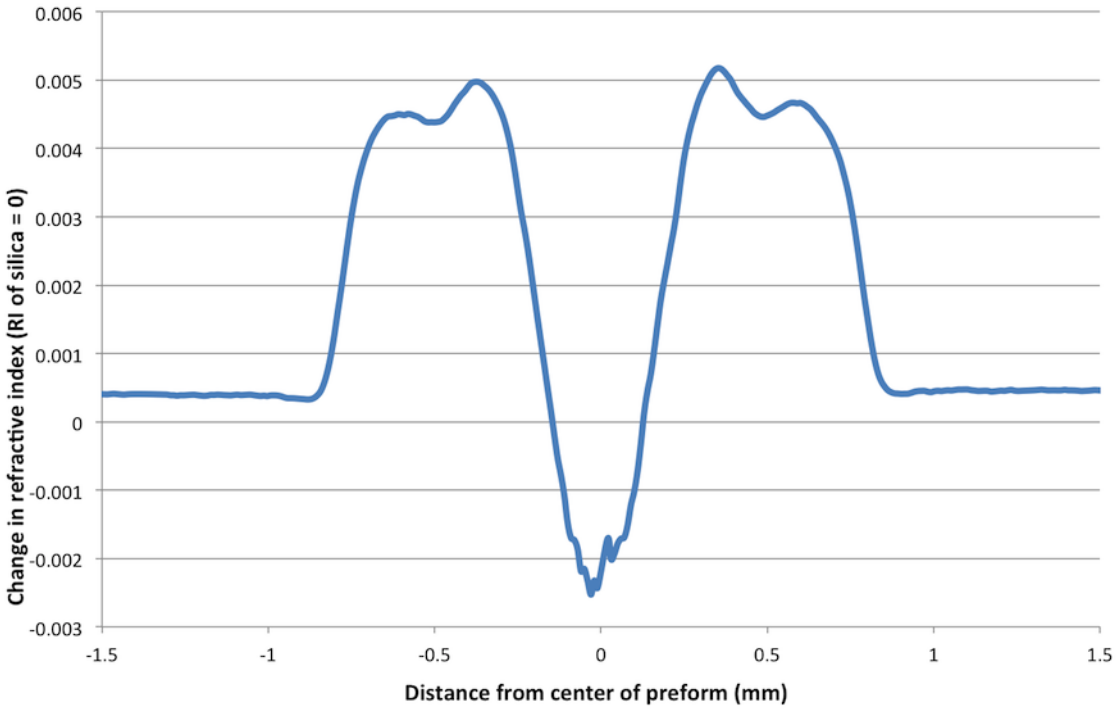

Figure 2.3: Refractive index profile of the core used to draw the initial longitudinally gradient fiber.

Figure 2.4: Core slug from initial preform. Note that the core does not extend across the entire diameter of the slug.

silica cladding tube (either Fluosil or F320, as will be discussed in greater detail below), which then were sleeved inside a 10 mm inner diameter by 26 mm outer diameter F300 silica tube (Hereaus, Buford, GA). The fluorinated silica inner cladding tube provides a lower refractive index relative to the longitudinally-graded core slug, in both doped and un-doped regions, to enable light-guiding in the resultant fiber. The outer pure silica cladding tube, though not necessary in theory, was employed since fluorinated silica tubes with the desired core/clad ratio were not available. Pure silica rods, whose diameter matched well the inner diameter of the fluorinated silica inner cladding tube, were placed above and below the doped-SiO_2 core slug in order to make the entire fiber waveguiding and to more easily identify the regions of interest. The end faces of the silica rods and core slugs were polished with 30 μm and 5 μm grit polishing pads. In order to prevent motion and sagging of the individual pieces of glass comprising the preform during fiber fabrication, the entire billet was consolidated at about 2300°C on the lathe under a vacuum of roughly 1.5 inches of mercury.

As noted above, the side-core-drilled slugs were sleeved inside either a Fluosil or F320 (Hereaus, Buford, GA) cladding tube to enable waveguiding. Both Fluosil and F320 can be made with a range of fluorine doping levels and, concomitantly, refractive indices. For those employed here, the Fluosil and F320 inner cladding tubes had refractive indices that were 0.0058 and 0.001 below that of silica, respectively. Two otherwise identical preforms were constructed, one from each type of fluorinated silicate (Fluosil and F320) glass in order to control the numerical aperture and determine to what extent this influenced the fabrication and performance of the fiber. The fully-consolidated preforms, of 25.7 mm (containing the Fluosil) and 27.06 mm (containing the F320) total diameter, were drawn on a Heathway optical fiber draw tower (Clemson University) at a temperature of about 1950°C to a 125 μm diameter fiber. The fibers were coated with a standard single coating (Desolite 3471-3-14,

DSM Desotech Inc., Elgin, IL) to a final outer diameter of about 235 μm. The total length of fiber drawn was nearly 1700 m, which was done to ensure that the entire longitudinally-graded core region was drawn. It was found that after consolidation, the Fluosil preform had developed small bubbles around the core, the result of fluorine outgassing from the glass. As a result, the fiber was unable to guide light; however, it was still usable in terms of determining germania content along its length, which was the primary goal at this stage. The preform using F320 as cladding glass consolidated without any such flaws. As such, all subsequent preforms were manufactured using F320 cladding in a silica tube.

Electron microscopy of selected preform and fiber samples was performed using a Hitachi S-3400 scanning electron microscope (SEM) operating at 20 kV under variable pressure and a working distance of about 10 mm. Elemental analysis was conducted using a Hitachi TM-3000 tabletop electron microscope operating at 15 kV.

Chemical composition of the initial LGF was determined by Energy dispersive X-ray spectroscopy (EDX or EDS), an analytical method that uses X-rays or high-energy electrons to excite electrons to higher energy levels. Upon returning to the ground state, the electrons emit X-rays that are characteristic to their respective elements. Fiber samples were first subjected to approximately 30 EDX point scans (scans which give the chemical composition at a selected point). Placement of the points ensured the center of the fiber and surrounding areas were scanned. Point scans were set to collect data for 35 seconds per data point. After all point scans for a sample were completed, a map scan of the entire surface of the cross-sectional area of the fiber was allowed to run for approximately 15 minutes. Fiber samples were taken in 10 m increments. On subsequent draws samples were taken in 20 m increments in order to decrease the time required to find the region of interest. When the doped core was found (i.e., germania was detected) an additional 5-7 point scans

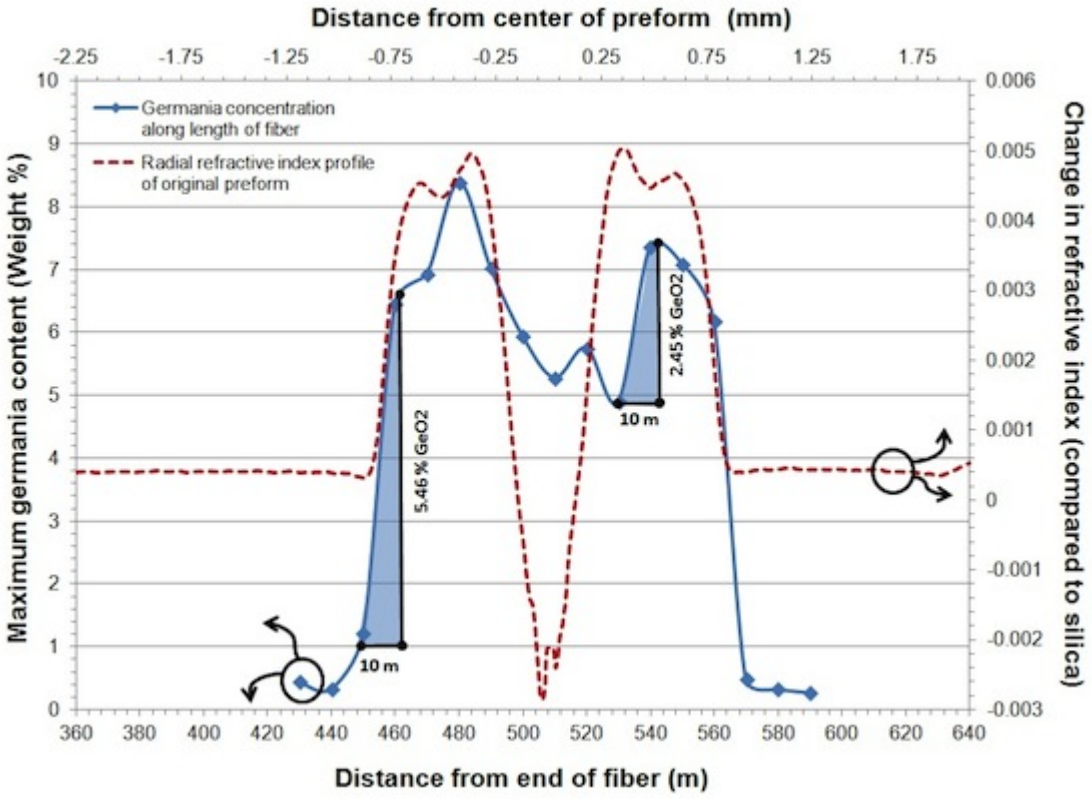

Figure 2.5: Refractive index profile of the as-made MCVD preform at the position where the core slug was side-drilled out (dashed red line) and the average germania [GeO_2] concentration in the core measured at a variety of positions along the length of the as-drawn fiber (solid blue line; specific data points shown as diamonds). Note that the germanium content along the length of fiber follows the refractive index of the as-made preform. The circles and arrows denote the corresponding ordinate and abscissa for each curve. Also provided, in the shaded areas, are examples of length-wise GeO_2 gradients in the as-drawn fibers of about 0.55 and 0.25 weight % GeO_2/meter.

were conducted on the core. The data shown here represents the maximum germania content measured.

A comparison of the refractive index of the original core and the longitudinal change in germania content is shown in figure 2.5. Spectral attenuation measurements were conducted on the fiber drawn using F320 cladding using a cut-back method on a Photon Kinetics PK2500 (Beaverton, OR) over a range from 850 nm to 1700 nm in approximately 5 nm steps. The refractive index profile at arbitrary position along the length of the fiber was measured at 980 nm by Interfiber Analysis Inc. using a spatially resolved Fourier transform technique [73] in which the fiber is placed transversely in the sample arm of a Mach-Zehnder interference microscope and a translating wedge is used to introduce a known phase shift between the two interferometer arms. The uncertainty in the measured refractive index value is no greater than $\pm 1 \times 10^{-4}$ based on comparisons with NPL reference fiber. However, for most situations, i.e., conventional core sizes and index differences relative to silica, $\pm 1 \times 10^{-4}$ is a conservative upper bound with $\pm 2 \times 10^{-5}$ more likely [74].

The experimental apparatus used to measure the Brillouin gain spectrum (BGS) is a heterodyne system [75] similar to that described in [76]. In short, the system launches a narrow-linewidth signal at 1534 nm through a circulator and into the fiber being tested for which a measurement of the BGS is desired. The Stokes signal generated in the test fiber passes back through the circulator and is analyzed with a heterodyne receiver. A characteristic signature from the circulator fiber is typically observed in the measured spectra. The system utilized for these experiments has been slightly modified over figure 2 of [31] for improved sensitivity. In this case, specifically, a fiber Bragg grating-based tunable band-pass filter was inserted after the final fiber amplifier stage, and was centered at the testing wavelength. One additional fiber amplifier stage was used to boost the signal level before launch into

the photo-receiver. As a control, a standard single mode fiber (SMF-28^{TM}, Corning Incorporated) was used. SMF-28^{TM} has approximately a silica core doped with about 4 mole percent GeO_2 ($\sim$6.7 weight percent GeO_2), yielding a core index difference with respect to the cladding of about 5×10^{-3}, and a core diameter of about 8.2 μm.

2.1 Longitudinally Uniform Refractive Index Preform

As explained in Chapter 1, one method of suppressing SBS is by varying the acoustic profile of the fiber. In this step, two core layers with significantly differing chemical compositions were deposited. The preform used was approximately 475 mm long with an inner diameter of 19 mm and an outer diameter of 25 mm. The larger preform tube was used to allow for a greater mass of soot to deposit during production and consequently, a larger core resulting after collapse. Fabrication was performed in a similar manner as previously described with two alterations. First, the number of core layers was reduced to two to decrease core complexity and more easily determine the properties of the two cores. The first (outer) layer was comprised of silica and germania with the respective precursor gases $SiCl_4$ and $GeCl_4$ flowing at 40 sccm and 80 sccm. Seven deposit passes were done for this layer to increase soot and, by extension, core thickness. The inner core layer had a higher germania content that was balanced with fluorine for index depression. The precursor gases in the inner core were flowing at 90 sccm ($SiCl_4$), 100 sccm ($GeCl_4$), and 30 sccm (SiF_4). The refractive index profile for the resulting preform at various locations si shown in figure 2.6. The second alteration from the previous preform was a step added to the process for solution doping prior to consolidation of the outer core layer.

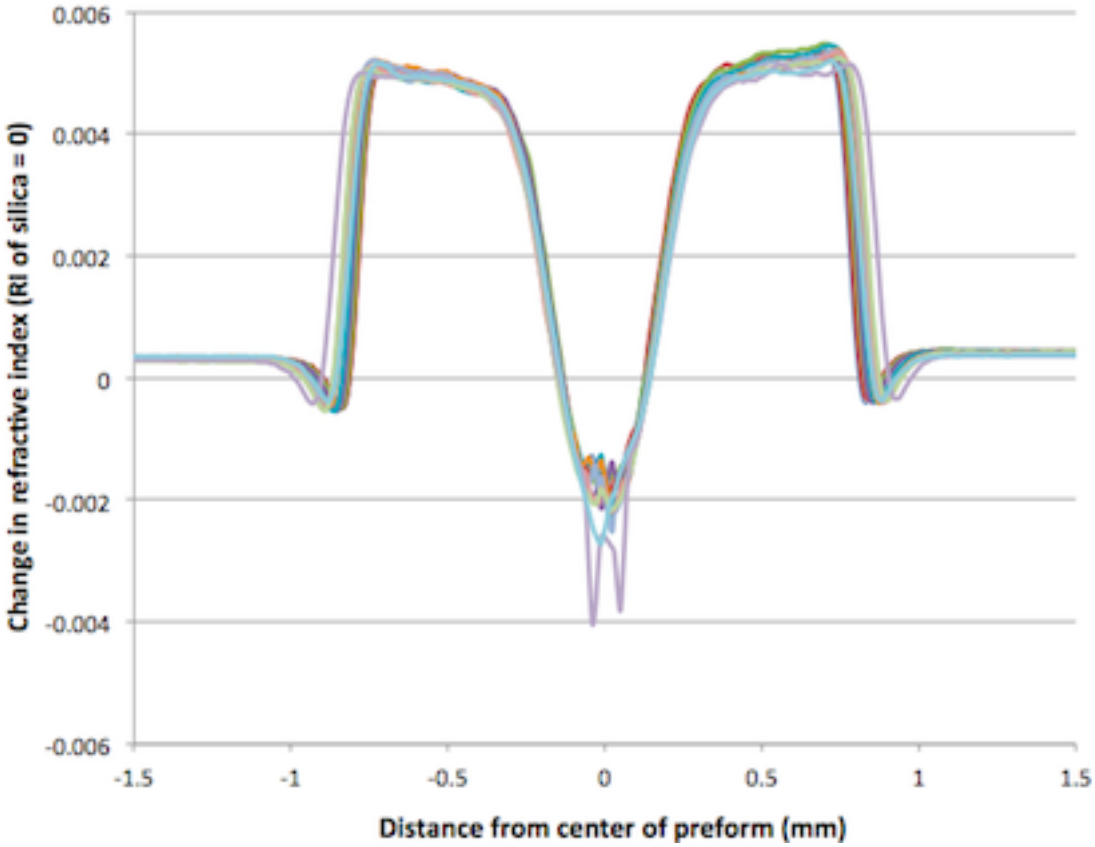

Figure 2.6: Refractive index profile of the longitudinally uniform refractive index core preform as measured at various locations along its length. The refractive index changes by approximately -0.0002 from the outside to the beginning of the central dip.

Rods of about 2 mm diameter (smaller diameter than the core slugs drilled from the original preform) were core-drilled through the full diameter of the preform (Ceramare, Piscataway, NJ) and sleeved inside a F320 fluorinated silica cladding tube The consolidated preform was drawn under the same parameters as the previous preform.

An attempt was made to dope the outer core layer with ytterbium, but after the perform was completed, it was found that the solution used was too weak and thus usable amounts of ytterbium were not incorporated into the glass. During the drying

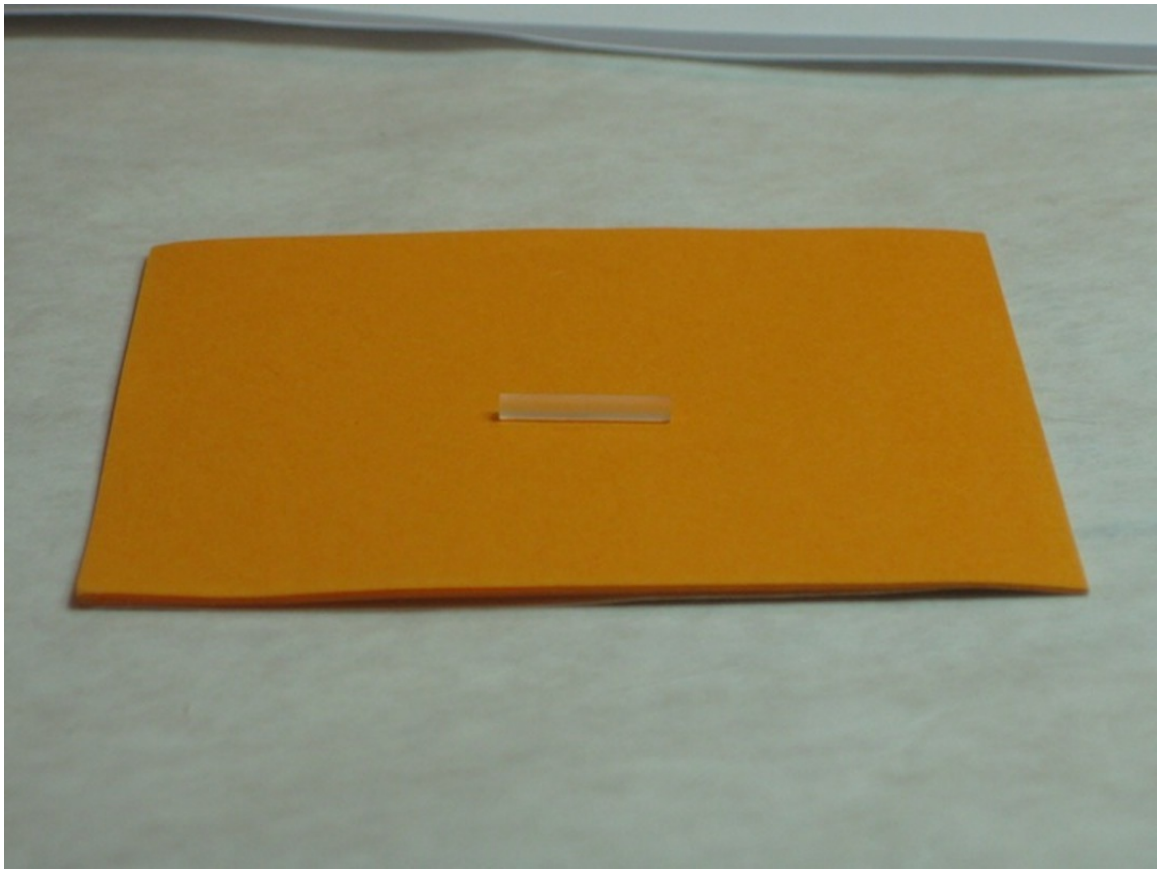

Figure 2.7: Photograph of a representative core slug drilled from the flat-index core preform.

steps, it was found that fluorine had been flowing through the tube and may have been incorporated into the soot, influencing the refractive index of the outer core as it had not yet been sintered. Regardless, because the two layers had distinct, different chemical compositions regarding silica and germania and because the refractive index profile was flat across the entire core width, it was decided to continue work with the resultant preform.

After fabrication, the preform was core-drilled (Cidra Precision Services, Wallingford, CT). The resulting slugs were 2 mm in diameter and approximately 12 mm in length. While showing improved surface quality when compared to the previous core

slugs (figure 2.7), the surface was still not pristine. When looked at down their length, it became evident that the cores were not perfectly circular, the result of the slugs being drilled off-center from the preform. Thus, semi-circular core shapes were produced during subsequent draws.

2.2 Ytterbium Doped Preform

The final preforms produced were doped with Yb^{3+} (sourced from 99.9999% purity $YbCl_3 \cdot 6H_2O$) to produce active fiber. The substrate tube used was approximately 450 mm in length with an inner diameter of 19 mm and an outer diameter of 25 mm. This preform was engineered to have two core layers of varying chemical composition. The outer core was produced by a single pass using $SiCl_4$ $GeCl_4$ flow rates of about 400 sccm and 80 sccm, respectively. The inner core layer was deposited in five passes of lower gas flows. $SiCl_4$, $GeCl_4$, and SiF_4 were run at rates of 88 sccm, 100 sccm, and 25 sccm, respectively. The addition of fluorine was meant to counteract the increased proportion of $GeCl_4$ compared to $SiCl_4$. A solution doping step was conducted after the deposition (but prior to consolidation) of the first core layer. The second (inner) core layer was not doped. Additionally, the outer layer was made thicker to ensure that a larger proportion of the core contained Yb^{3+}. The solution used was made with 0.015M $YbCl_3$ and 0.30M $AlCl_3 \cdot 6H_2O$ for a total volume of 250 ml. The solution was co-doped with aluminum to increase the solubility and prevent ion clustering of the rare earth, without which decreased nonlinearity by cross relaxation would have resulted [77], [78].

Doping followed standard solution doping technique [79], [80], [81]: during preform production, after soot deposition but prior to consolidation, the preform was removed from the lathe and the solution was slowly pumped into the preform

with a peristaltic tube pump. Once the soot was completely saturated in solution, the preform was left to soak for one hour, after which time the solution was slowly drained from the preform. The preform was allowed to dry overnight in a low flow ($\sim$ 5 l/min) nitrogen atmosphere before being returned to the lathe and further dried under an atmosphere of oxygen, helium, and chlorine, with the oxy-hydrogen burner at a low temperature. The soot was then consolidated and preform production finished as per usual MCVD operation. Before collapse, a second soot layer was deposited with fluorine to counteract higher levels of germainia. Due to the presence of aluminum and ytterbium ions, the refractive index of the outer layer was elevated beyond what would be expected from germania alone. Time constraints prevented further optimization of the design to produce a preform with an invariant refractive index profile across the two core layers. The refractive index profile of the final preform can be seen in figure 2.8.

While other methods of incorporating rare earths into fiber preforms have been reported [82], [82], [83], solution doping remains standard due to its versatility and ease. Numerous rare earth ions have been used in fiber fabrication, including erbium [84], praseodymium [85], neodymium [86], and ytterbium [87]. Erbium is the most commonly used active fiber dopant because it emits at wavelengths commonly used in telecommunications [88] and has high quantum efficiency up to $\sim$ 7 wt%, the upper limit of erbium incorporation before ion clustering becomes unavoidable [89]. For this thesis, ytterbium was chosen as the dopant due to a wide variety of beneficial optical properties beyond communications. Historically, ytterbium has been used primarily in lasers [90], but more recently have found applications as fiber amplifiers [91]. The benefits of ytterbium when compared to erbium include broad absorption and emission bands ($\sim$ 975 nm - $\sim$ 1200 nm), high output power and conversion efficiency, long lifetimes (on the order of 1 ms), and a simple energy diagram; the

ground state $^2F_{7/2}$ and excited state $^2F_{5/2}$, separated by about 10,000 cm^{-1}, are the only energy levels associated with ytterbium pumping. [92], [93], [94].

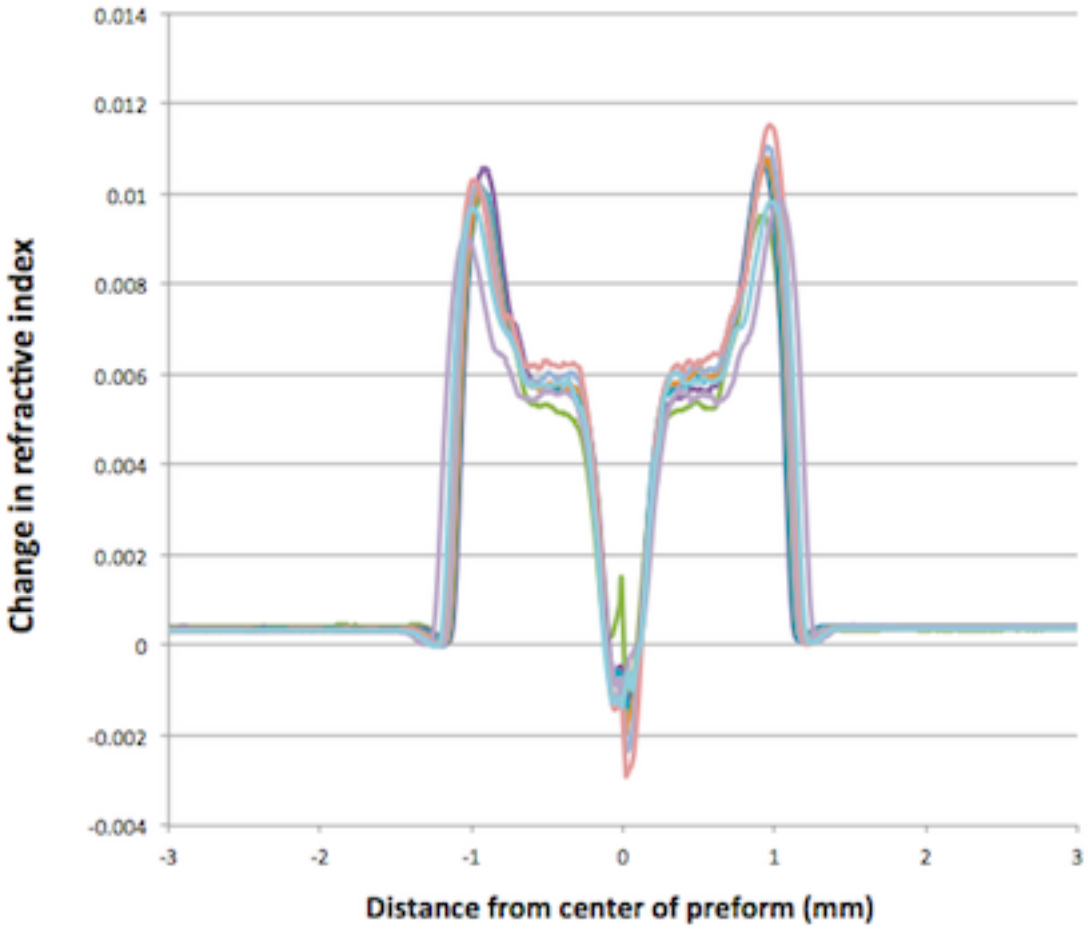

Figure 2.8: Refractive index profile of the longitudinally uniform refractive index core preform as measured at various locations in 10 mm increments along its length. The outer and inner core layers can clearly be distinguished by the varying refractive indecies.

Chapter 3

Results and Discussion

3.1 Optical Properties

The correlation between the radial refractive index profile from the original preform and the average germania concentration along the length of the longitudinally-varying optical fiber is shown in figure 2.5. There are several different longitudinal gradients in this particular fiber as a function of length. Emphasized in figure 2.6 are two such gradients where the measured GeO_2 content changes by 5.46 % or 2.45 % over a 10 meter length yielding gradients of 0.546 %/m and 0.245 %/m, respectively. These values are higher by a factor of about 1900 times the gradients achieved in [17] by virtue of the fact that the compositional gradient is built into a smaller region of the preform and not the entire rod.

There are several points of interest in figure 2.5. The central dip in the index profile of the original preform results from burn-out of the germania and fluorine. The use of fluorine during the collapse of the original preform leads to the negative index values, relative to pure silica, that are observed. Additionally, while the GeO_2 level in this fiber is higher than that in SMF-28^{TM} ($\sim$ 8.4 versus 6.7 weight percent),

the fluorine co-doping yields an index difference that is essentially equivalent (+0.005 relative to pure silica).

Figure 3.1 provides the refractive index profiles, relative to silica and measured at 970 nm, at two different locations over an arbitrarily chosen 20 m length of the LGF. As can be seen, the index difference changes by about 0.001, representing a numerical aperture change of 0.013 ($\sim$ 13%), over a distance of only 16.6 m, verifying that the fiber indeed possesses a gradient in refractive index along its length. The numerical aperture, NA, governs the modal properties of the fiber. For the fibers developed in this work, minimum NA is defined by the fluorinated silica inner cladding and the pure silica ends of the side-core-drilled slug. Accordingly, the NA is 0.054 for these pure silica core lengths of fibers drawn using the F320 inner cladding tube. The maximum NA then would be defined by the fluorinated silica inner cladding relative to the refractive index associated with the maximum germanium content portion of the longitudinally-varying optical fiber. Accordingly, for this specific fiber, the maximal change in numerical aperture is 0.067 (0.120 maximum versus 0.054 minimum).

The lowest loss of the LGF was 82 dB/km at a wavelength of 1550 nm (figure 3.2). Thus, there would be less than 1 dB of loss over a 10 m segment where the germania gradient is greatest. A very large hydroxyl ion absorption peak was observed at 1380 nm indicating water contamination, likely due to the wet-cutting and grinding of the core-drilled slugs that then were re-sleeved into the fluorinated cladding tube. Regardless of source at this proof-of-concept level, the measured losses are dominated by extrinsic factors since the spectral attenuation of the as-prepared (prior-to-side-core drilling) original preform had a minimum value of about 23 dB/km at a wavelength of 1550 nm.

Since material composition influences both the optical and acoustic properties of the fiber, Brillouin gain spectra (BGS) were measured from both ends of the same

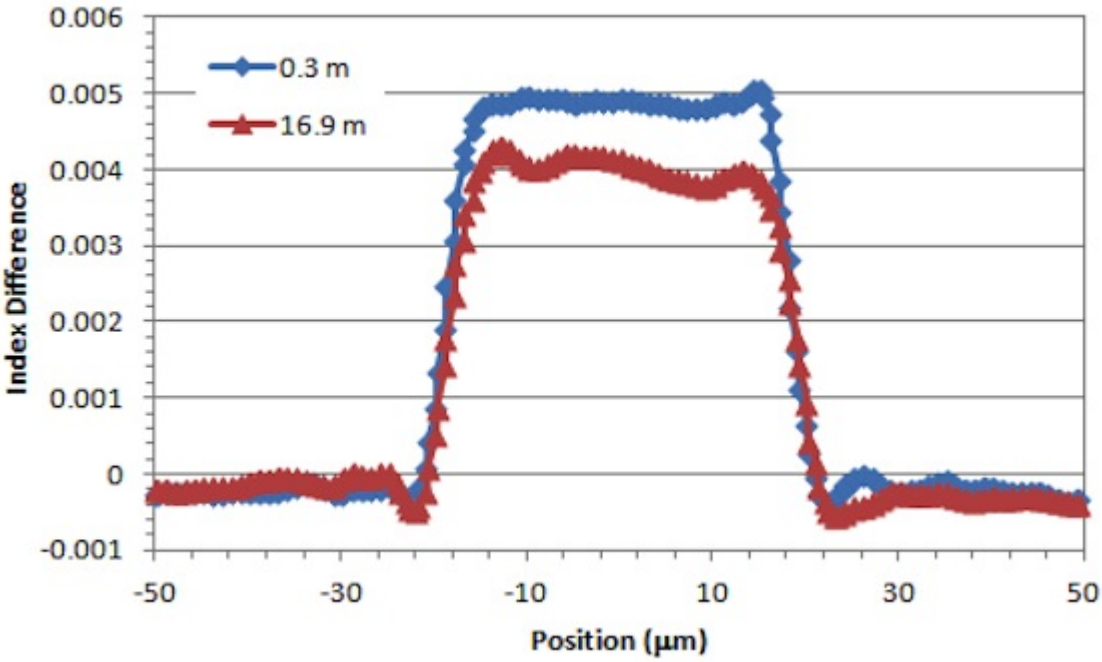

Figure 3.1: Refractive index profiles at 0.3 and 16.9 m positions along a 20 m length of the longitudinally-graded optical fibers. Profiles were taken at a wavelength of 970 nm.

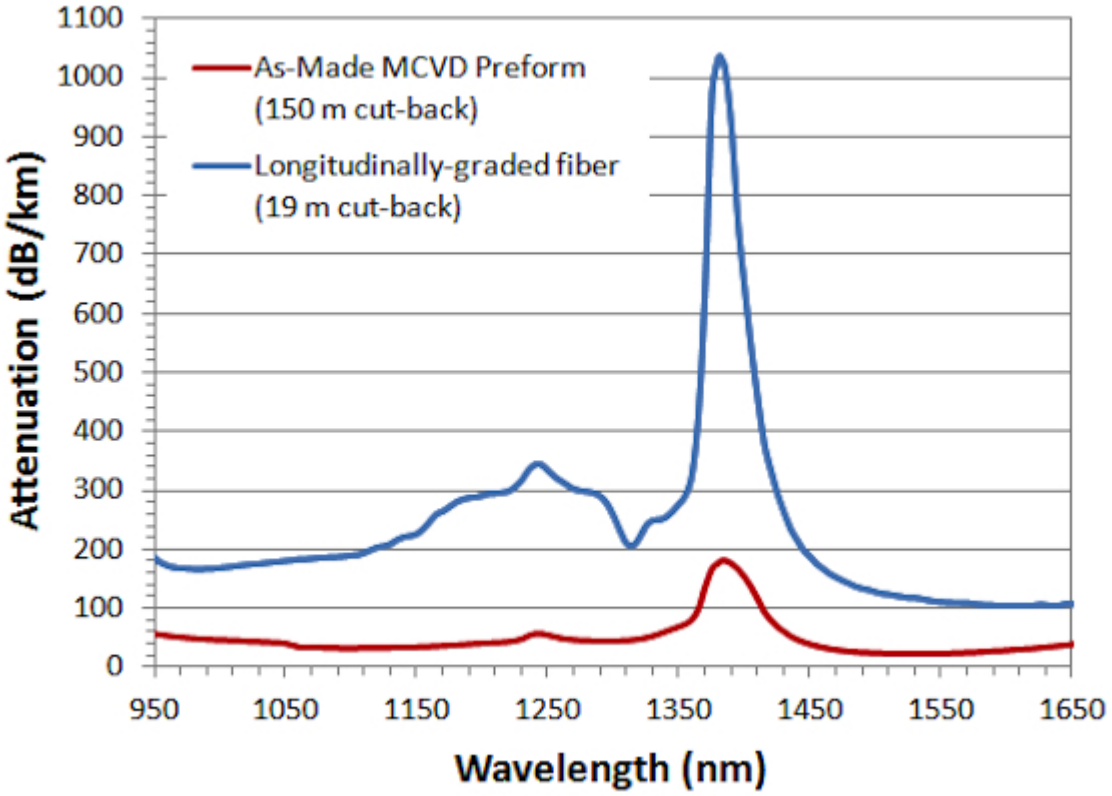

Figure 3.2: Spectral attenuation of the longitudinally-graded optical fiber and the as-made original MCVD preform. The minimum loss of the longitudinally-graded fiber was about 82 dB/km, whereas for the original preform, the minimum loss was about 23 dB/km.

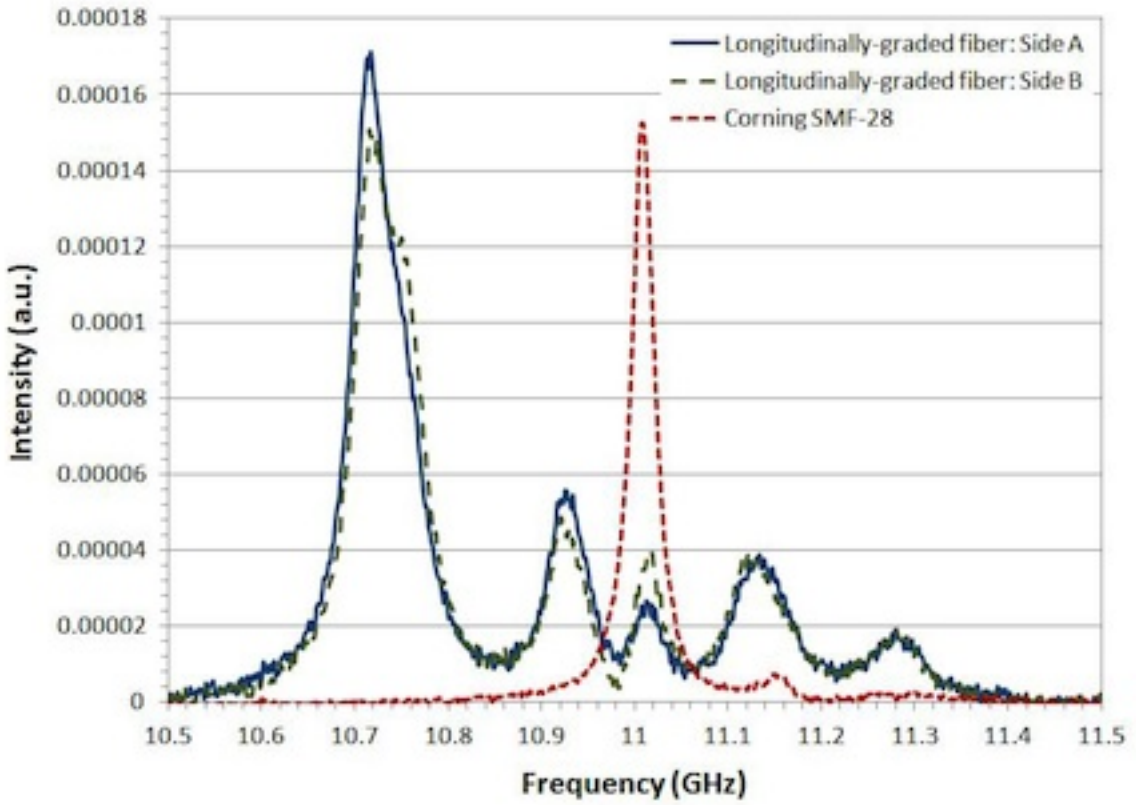

Figure 3.3: Stimulated Brillouin scattering spectrum of the longitudinally-graded fiber, interrogated from both ends (arbitrarily A and B), and a conventional single mode fiber (Corning SMF- 28TM) measured at a wavelength of 1534nm.

length of the LGF (ends arbitrarily designated as A and B) and compared to that from a conventional (Corning SMF-28^{TM}) optical fiber. The results are shown in figure 3.3. The LGF spectra are normalized roughly to the highest-frequency peak, with reasoning to be discussed later. The multiple peaks observed in the LGF are believed to be modes of the acoustic waveguide and the peak near 11 GHz is a contribution by the measurement apparatus.

Due to the background loss at the test wavelength ($\sim$ 80 dB/km), there is slightly less pump power to drive Brillouin scattering from the fiber end opposite (far-end) the optical launch end (near-end). The back-scattered Stokes signal from the

far-end also experiences more total loss than the signal scattered from the near-end. Thus, the Stokes signal from the far-end contributes less to the measured spectrum than that from the near-end, which can be used to explain the observed differences in the Side A and Side B measurements. Looking just at the L_{01} mode ($\sim$ 10.71 GHz), since there is relatively more signal at lower frequencies for Side A than Side B, it can be concluded that Side A has more GeO_2 than Side B. The structure in the spectrum probably results from a non-linear length-wise change in germania content in the test segment.

The measured spectral width (FWHM) of the SMF-28^{TM} fiber is about 29 MHz. In contrast, the spectral width (FWHM) of the LGF is approximately 80 MHz, representing a broadening by about 50 MHz, or increase of about 4.4 dB. In order to compare the Brillouin gain coefficients, the acousto-optic overlap integral (i.e., the relative strength of higher-order acoustic modes, or HOAMs) must be taken into account. There is only one weak HOAM (L_{02}) observed for the SMF-28^{TM}, whereas there is a significant presence of HOAMs in the LGF. Coarsely integrating the spectra such that the total integrated Brillouin gain is conserved [95], not including the contribution by the apparatus, the LGF has a Brillouin gain coefficient about 6.7 dB below that of the standard commercial single-mode longitudinally-invariant optical fiber. Additional detail, including a notional design for 10 dB SBS suppression, is provided in appendix A.

The presence of these modes is most likely due to perturbations from core circularity arising from the core-drilling process, and not from an intrinsic refractive-index dip usually associated with Ge-doped fibers. As noted above, the results on these initial fibers should be considered, at best, proof of concept. As with any nascent effort, much work remains towards achieving higher performance and complexity. The purpose of this section is to offer recommendations as to next steps, as well as potential

applications that could gain benefit from the findings of this work.

Even though a 20 m length of the LGF would only impose an added loss of $<$ 2 dB, further reduction in attenuation is warranted. The measured losses in the LGF (figure 3.2), with respect to the as-fabricated initial preform, likely result principally from the core-drilling and rod/tube stacking process. That said, the subsequent polishing of the core-drilled slugs was minimal and as such any improvement in surface quality, and therefore loss reduction, would be minimal. It is worth noting that a wide variety of specialty optical fibers used today employ core-drilling and stacking processes (e.g., boron stress rods in polarization-maintaining fibers, rod/tube stacking in photonic crystal, and microstructured optical fiber), and so these general processes are amenable to higher quality, lower loss fiber.

Additionally, it should be possible to both increase the gradient and change its longitudinal shape, both by enhanced doping and preform design. The present fiber exhibits a maximum germania gradient of 0.546%/m. Given the generalized process, higher doping levels within smaller core size initial preforms, sleeved inside narrower wall-thickness cladding tubes, would be effective in enhancing the gradient. Very high germania-content fibers have been fabricated using similar MCVD processes [96], and so significant opportunities exist for greater doping levels, hence greater longitudinal gradients (i.e., shorter LGF lengths). Additionally, multiple side-core-drilled slugs can be sequentially stacked atop one another in the secondary preform to permit one draw to yield multiple LGF sections. Further, if scaled to preform dimensions typical of commercial preforms ($>$ 300 mm [97]), then the same process would yield nearly 1 km of LGF.

3.2 Longitudinally Uniform Index Core

The longitudinally uniform index fiber, once drawn, resulted in $\sim$ 90 m of doped core. The maximum change in refractive index of the parent preform is approximately 0.0051, relative to silica. The change in chemical composition along the length of the fiber is shown in figure 3.4 and compared to the refractive index profile of the parent preform. The outer core layer has a slightly lower germania content. than the inner core; approximately 3.5 wt.% germania in the outer core layer compared to 4.1 wt.% germania in the inner core. The maximum germania content change along the fiber length is 0.228 wt.%/m and the fiber shows a maximum numerical aperture of 0.128. Between the two core layers germania content changes by 0.6 wt.%, or 0.003 wt.%/m. As with the original preform, the central dip in the refractive index profile is the result of fluorine incorporation and germania burnout during collapse.

A small section of the parent preform was cut and mounted for traditional drawing (i.e., invariant refractive index and composition along the fiber length). Spectral attenuation measurements were taken, the results of which can be seen in figure 3.5. The fiber shows a large absorption peak near 1375 nm indicating hydroxyl contamination, most likely from incomplete drying after a solution doping attempt. The fiber does show decreased loss compared to the initial LGF fiber, with a minimum loss of about 3.5 dB/km at 1525 nm.

The core drilling for this preform (Cidra Precision, Wallingford, CT), resulted in core slugs that were 2 mm in diameter and approximately 12-15 mm in length. The reduced diameter compared to the initial LGF core slugs was intentional, with the aim of ensuring the core of the parent preform took up the entire diameter of the core slug. The reduced diameter necessitated a change to the design of the LGF preform assembly. Namely, more layers of cladding glass (figure 3.6) were required to achieve

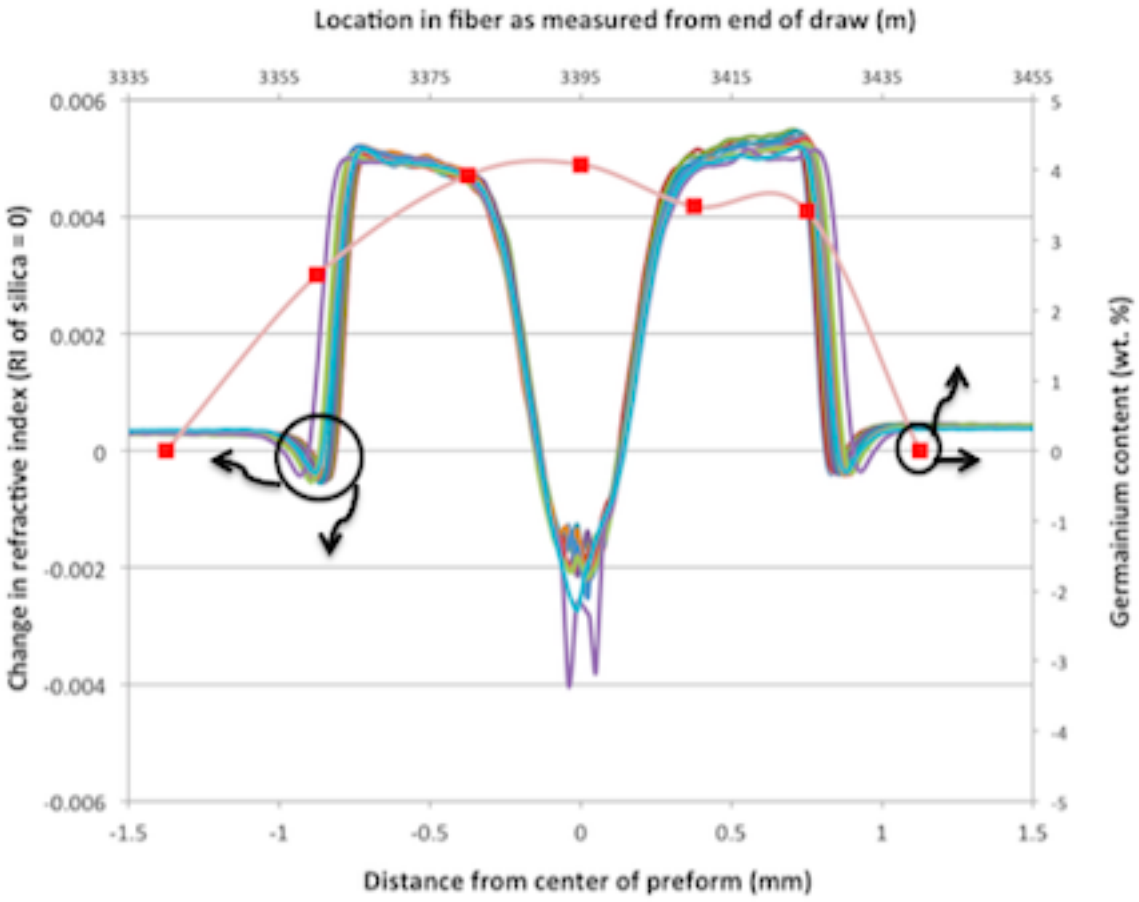

Figure 3.4: Refractive index profile of the as-made longitudinally uniform index preform at various locations (solid lines) and the average germanium [Ge] concentration in the core measured at a variety of positions along the length of the as-drawn fiber (red squares).

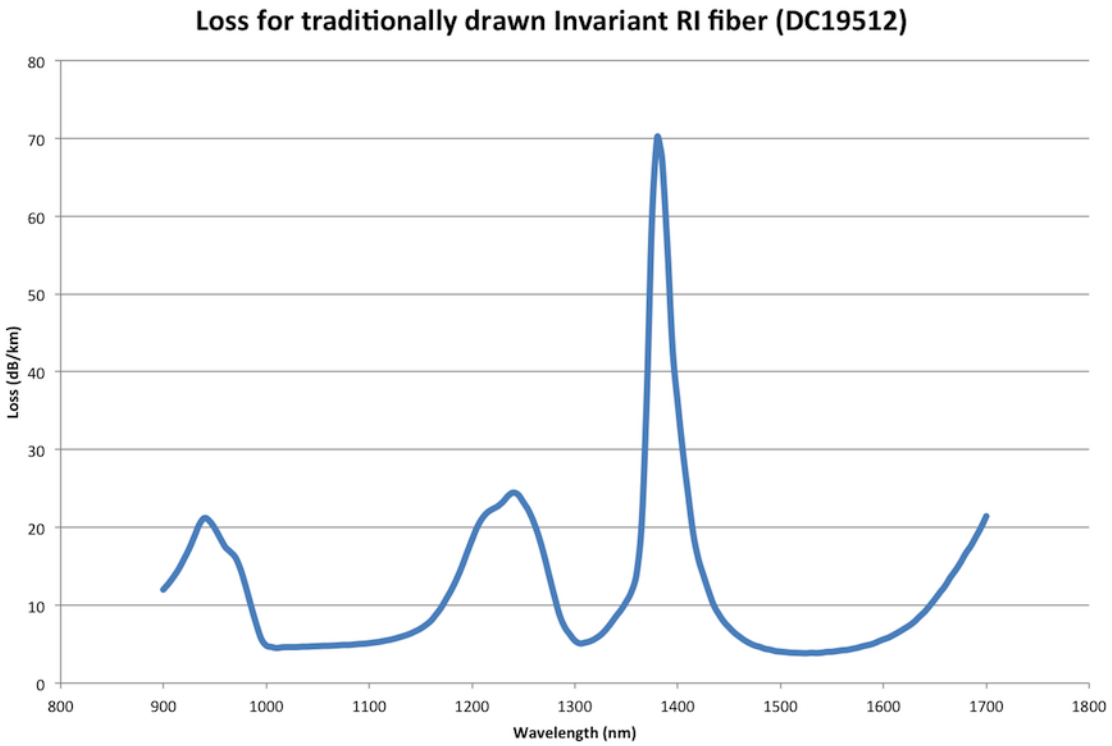

Figure 3.5: Spectral attenuation profile of the traditionally drawn RI-invariant preform.

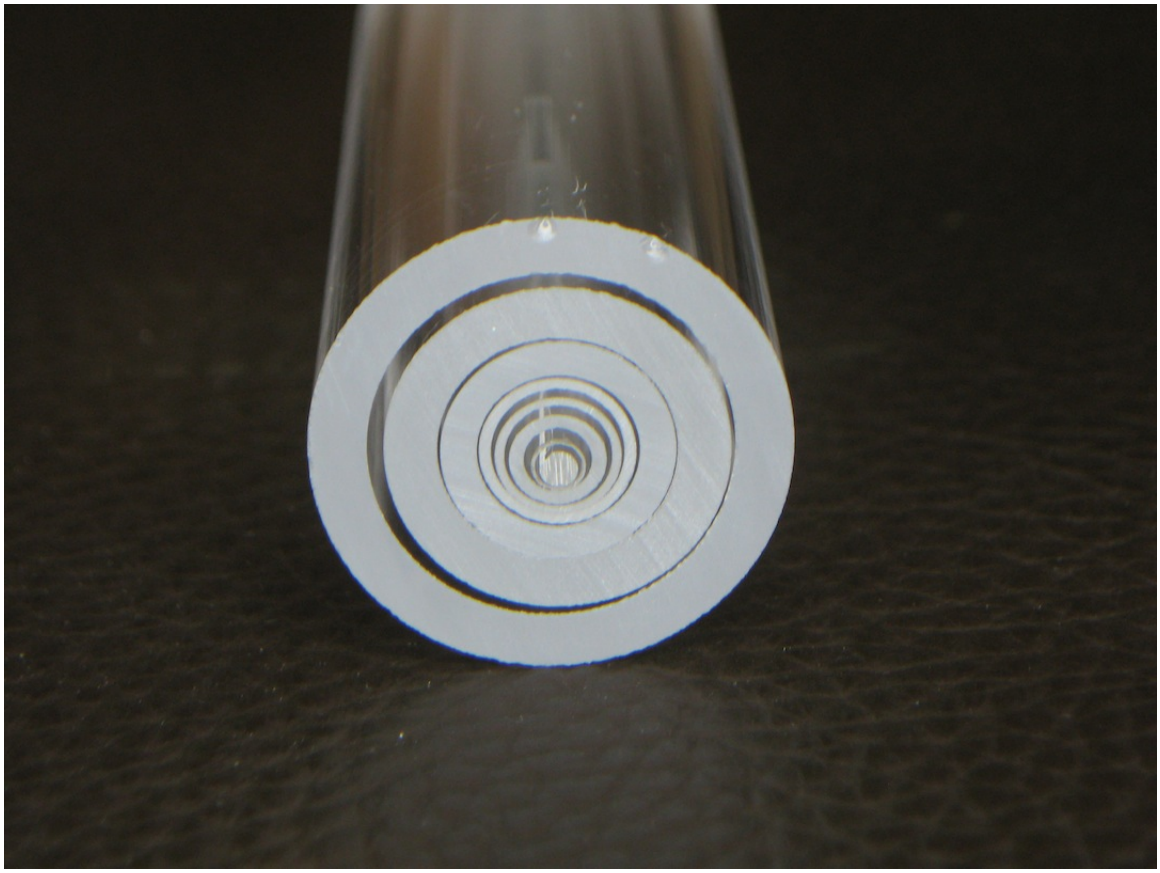

Figure 3.6: Image showing the increased number of layers of cladding glass required for the RI-invariant LGF preform. The same structure was used for the subsequent Yb^{3+} LGF preform.

the outer diameter required for single mode propagation. Other than this change in the number of cladding layers, the assembly and consolidation of the invariant-RI LGF remained the same as previously described. Unfortunately, the core slugs were drilled off-center from the centerline of the preform, resulting in semi-circular cores (figure 3.7). Due to their shape light was unable to guide and as a result, we were unable to conduct SBS and spectral attenuation measurements of the RI-invariant LGF.

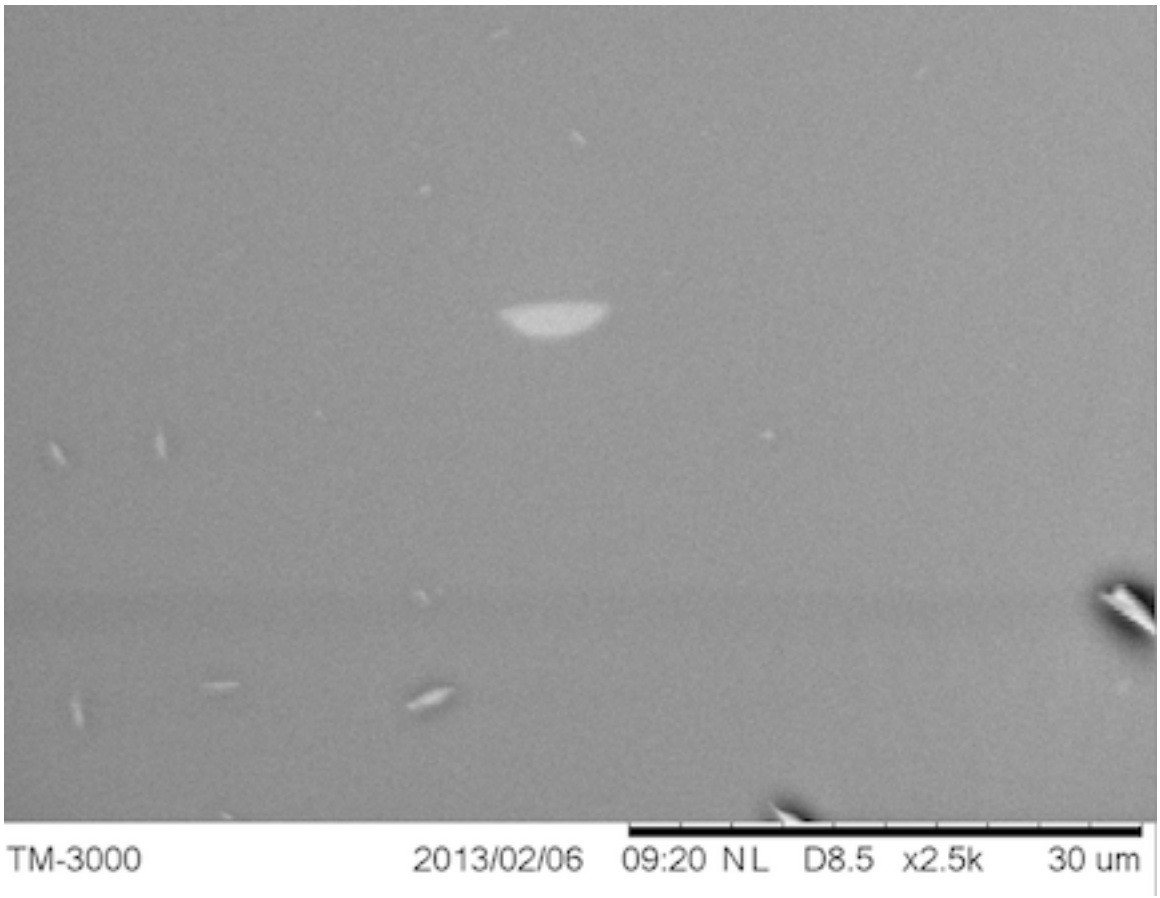

Figure 3.7: SEM micrograph of the core of the RI-invariant LGF showing the semi-circular shape of the core.

3.3 Ytterbium-doped fiber

The final preform was produced similarly to the RI-invariant preform in that there were two core layers of differing chemical compositions. While the intent was to again produce the same refractive index across the two layers, the addition of rare earth and aluminum ions increased the refractive index of the outer core and time constraints prevented altering the recipe to achieve an invariant refractive index between the two core layers. The refractive index profile and chemical composition data can be seen in figure 3.8. Again, the concentration of germania is shown to change along the length of the fiber and between the two core layers. The numerical aperture of the resulting fiber was 0.176, as measured from the peak refractive index and the germania content has a maximum longitudinally change of 0.15 wt%/m. The diameter of the core of the parent preform was 2.4 mm to ensure the entire diameter of the core was included in the core slug. Upon returning from core drilling, it was found that the core slugs were drilled over the center of the preform and did indeed contain doped core material along the entire diameter.

Attenuation in the fiber drawn from this preform was high in both the traditionally drawn fiber and the LGF (figure 3.9). The lowest loss measured in the traditionally drawn Yb^{3+} fiber was 88.4 dB/km at 1645 nm, while the lowest loss in the LGF fiber was 192 dB/km at 910 nm. The attenuation in the traditionally drawn fiber at 1550 nm was 121 dB/km, approximately 33 % higher than the initial LGF. The Yb^{3+}-doped LGF fiber showed 1494 dB/km loss at 1550 nm.

Both the traditionally drawn fiber and LGF fiber showed large levels of loss although the hydroxyl absorption peaks are not as intense (relative to the peak loss) as in previous fibers. Even though the preform core fully occupied the core slug, upon drawing it was found that although the cores were rounder than had previously been

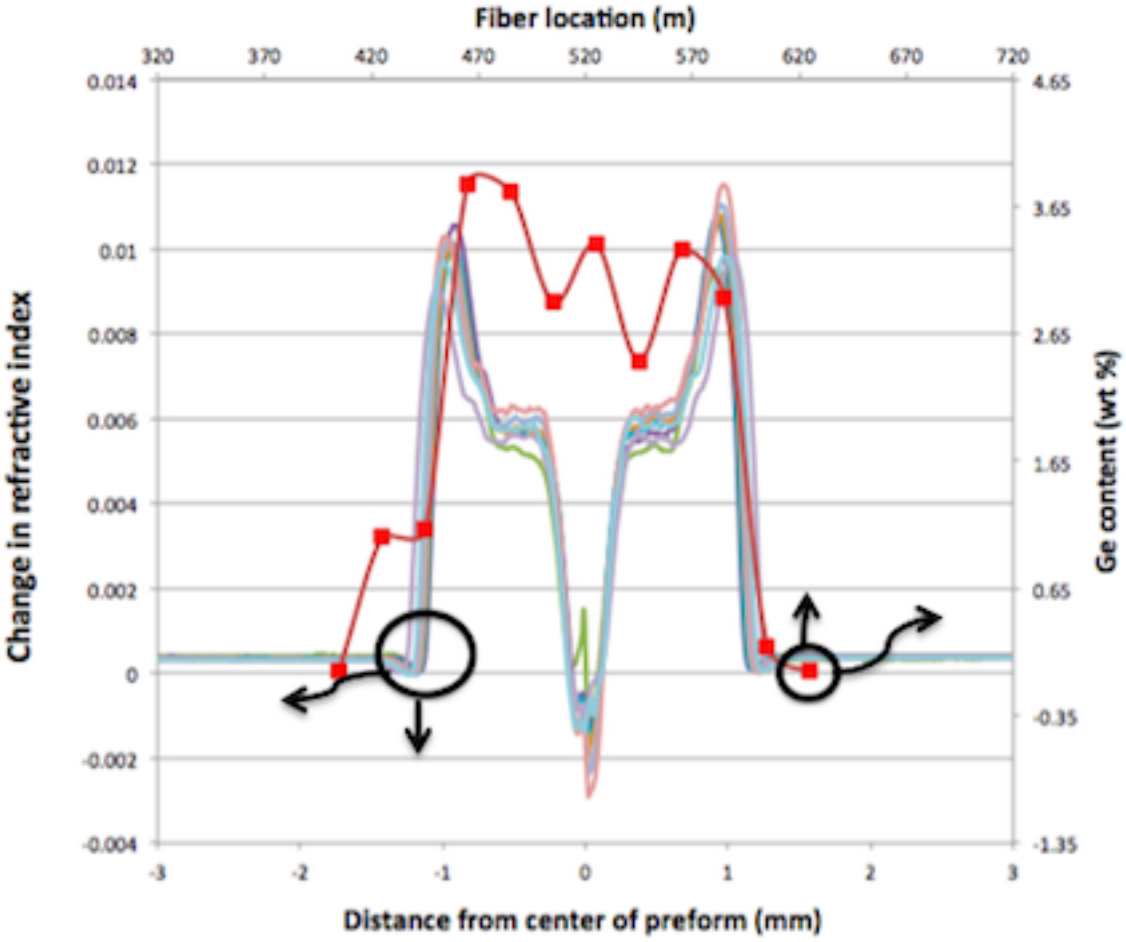

Figure 3.8: Refractive index profile of the parent Yb-doped preform and [Ge] content along the length of the resulting LGF.

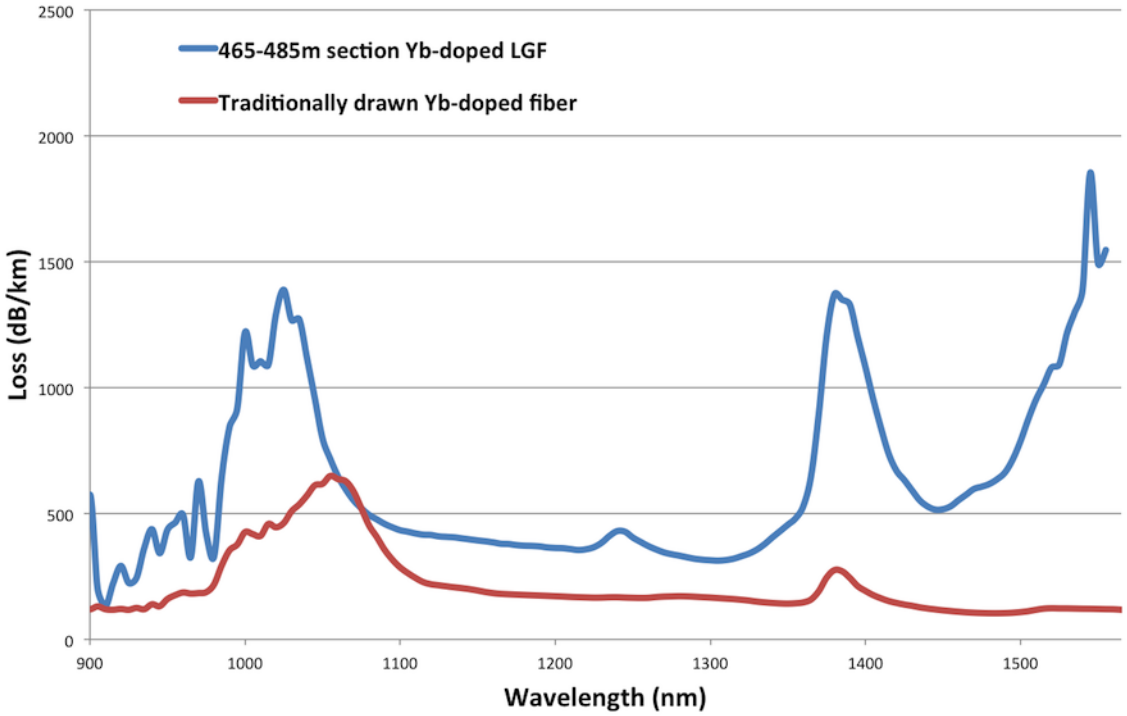

Figure 3.9: Spectral attenuation of a section of the Yb-doped fiber drawn traditionally (red) compared to a 20 m Yb^{3+}-doped LGF section (blue).

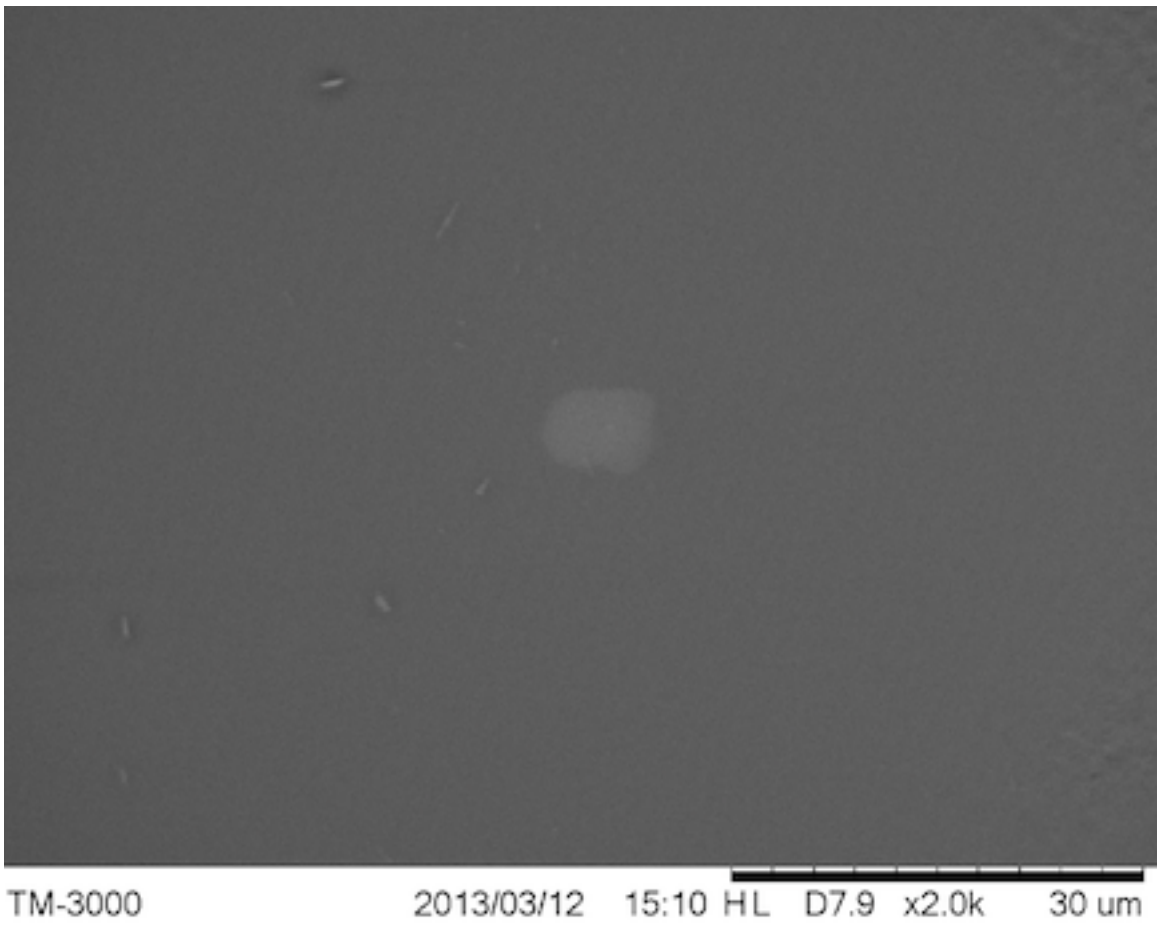

Figure 3.10: SEM micrograph showing the core at 465 m from the end of fiber collection.

seen, the core cross sections were not perfectly round (figure 3.10).

The Yb^{3+} LGF showed SBS suppression at least as good as the original LGF (figure 3.11). Due to high loss, single measurements could not be taken of the entire fiber, however measurements from both ends of the fiber characterizing different portions suggest that the Yb^{3+} LGF reduces Brillouin gain by at least 6 dB and as much as 8 dB. Full characterization of this fiber is still ongoing.

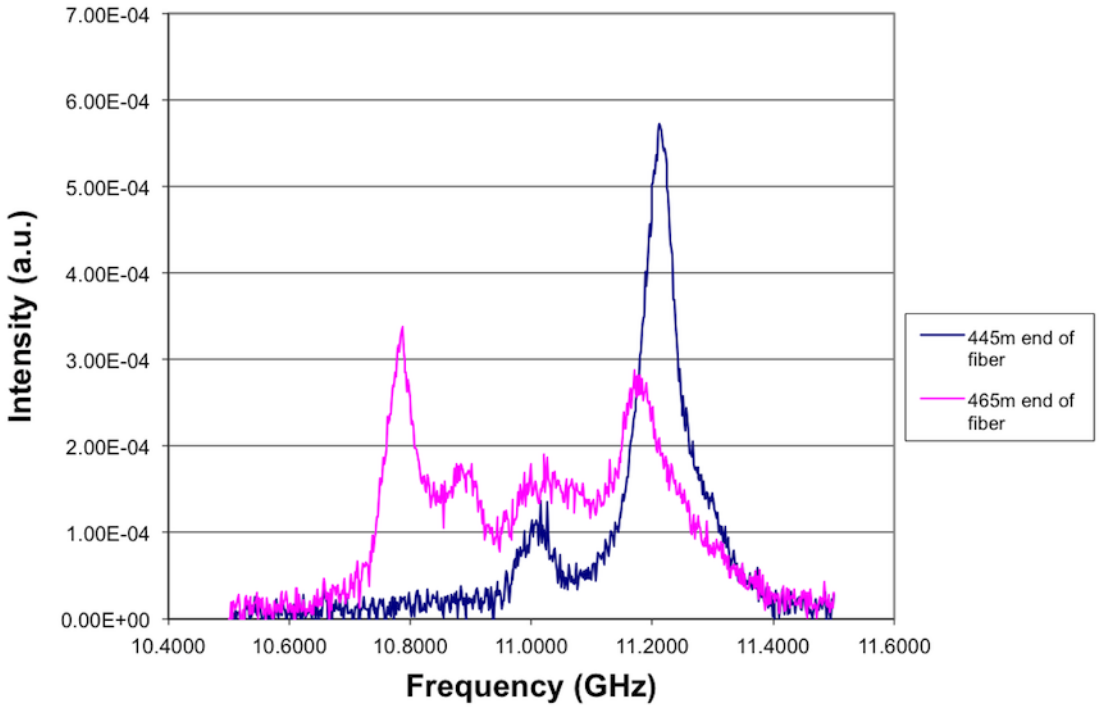

Figure 3.11: SBS spectrum of the Yb-doped fiber.

3.4 Rectilinear Core

Figure 2.4 provides a photograph of the actual side-core-drilled slug employed where the round core from the mother preform is clearly observed in the center surrounded by the extra cladding glass. Figure 3.12 shows a representative SEM micrograph of the resultant fiber cross-section with rectangular core. This approach yields fibers that possesses a dimensional change in core diameter and aspect ratio; a schematic of this is shown in figure 3.13. Given the circular cross-section of the initial MCVD-derived core within the side-drilled slug, the variation in the rectilinear core width, w, with distance drawn into the core, x, goes as $2 \cdot (1 - x^2)^{1/2}$; see figure 3.13 [d-e].

Figure 3.14 shows the measured refractive index profiles, taken at orthogonal directions about the cross-section, located seven meters apart at an arbitrary position along the drawn fiber. The aspect ratio of the core would be determined by the maximum aspect ratio of the slug that is side-drilled out of the initial preform and conceivably could take on a range of geometries. In the particular profiles shown in figure 3.14, the ratio between the full-width at half-maximum (FWHM) diameter of the major and minor dimensions are about 40 % [figure 3.14(a)] and 60 % (figure 3.6[b)], respectively. Further, as expected, based on the figure 3.13[c] schematics, one rectangular dimension does not change with position (figure 3.14[c]) while one does ([figure 3.14(d)]. Additionally, the average refractive index values change by about 5 % in both cases over the 7 m analyzed here proving that the fiber is both dimensionally- and optically-chirped with position along the fiber.

In order to further detail the change in core dimension with longitudinal fiber position, figure 3.15 provides several scanning electron micrographs of said core along a longer length of fiber ($\sim$100 m). In each image, the level of magnification is the

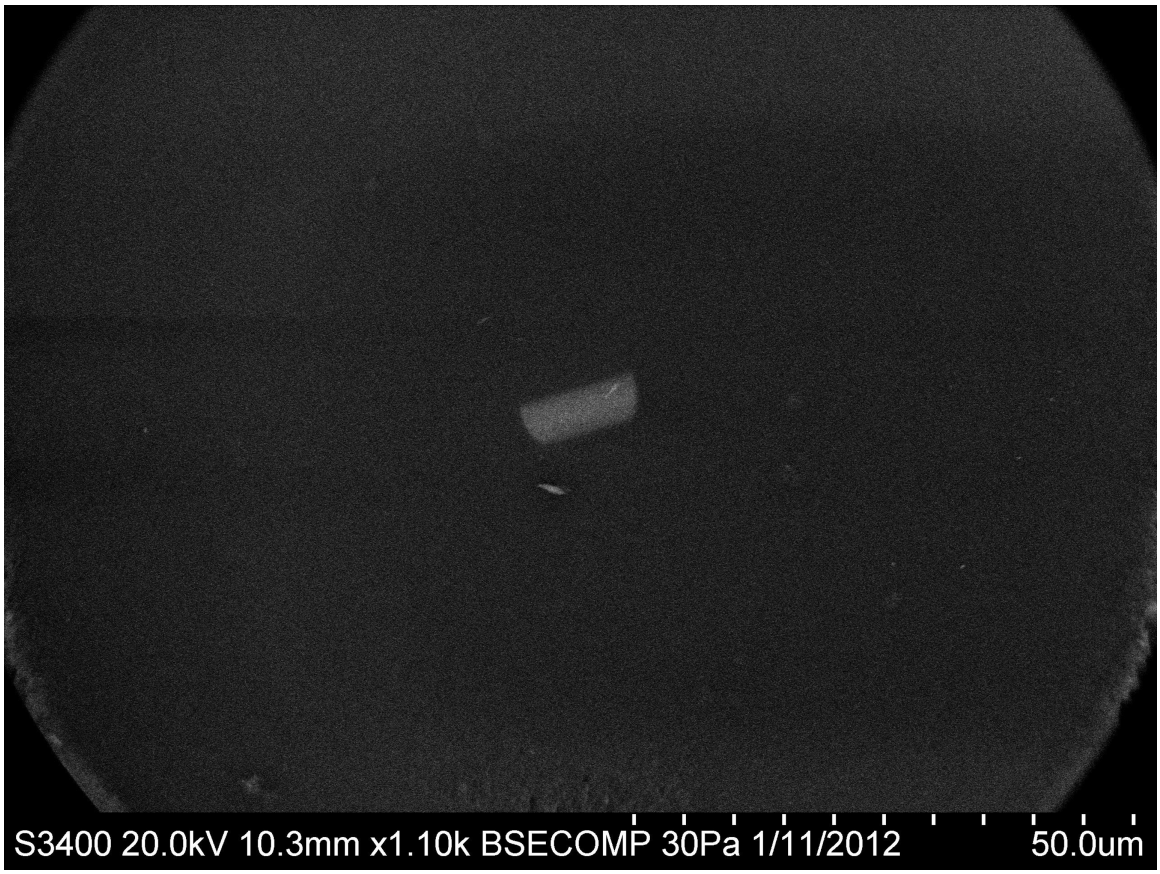

Figure 3.12: A representative SEM micrograph of the rectilinear core optical fiber.

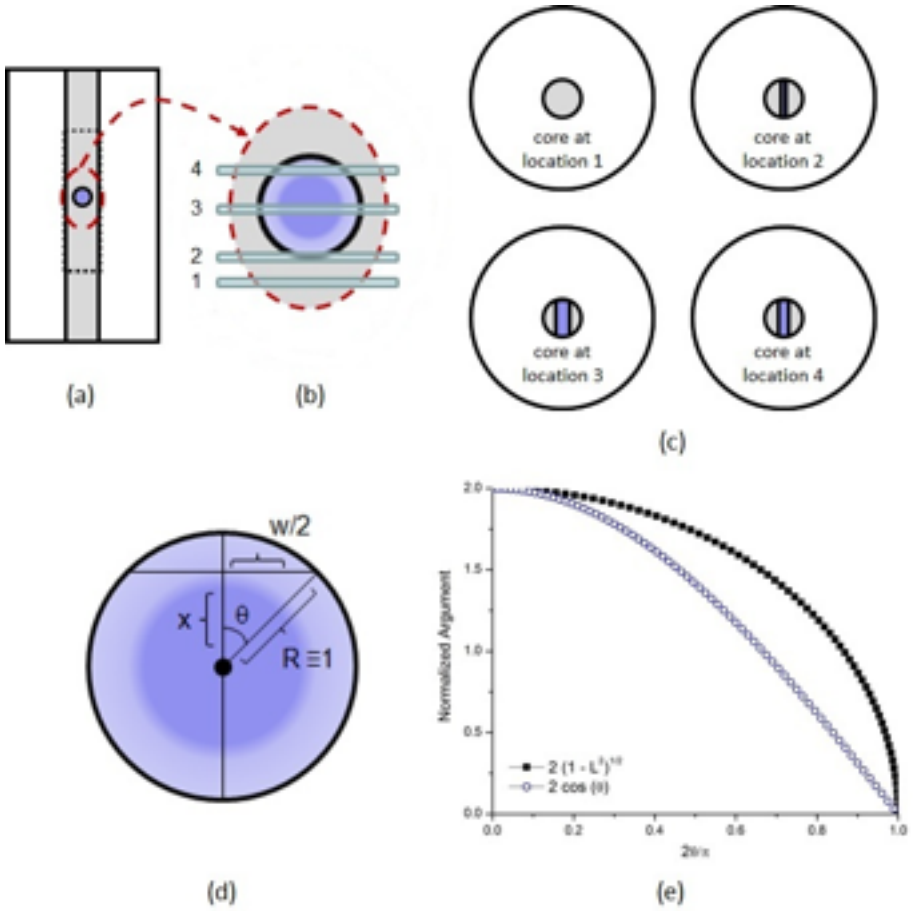

Figure 3.13: A representative SEM micrograph of the rectilinear core optical fiber.

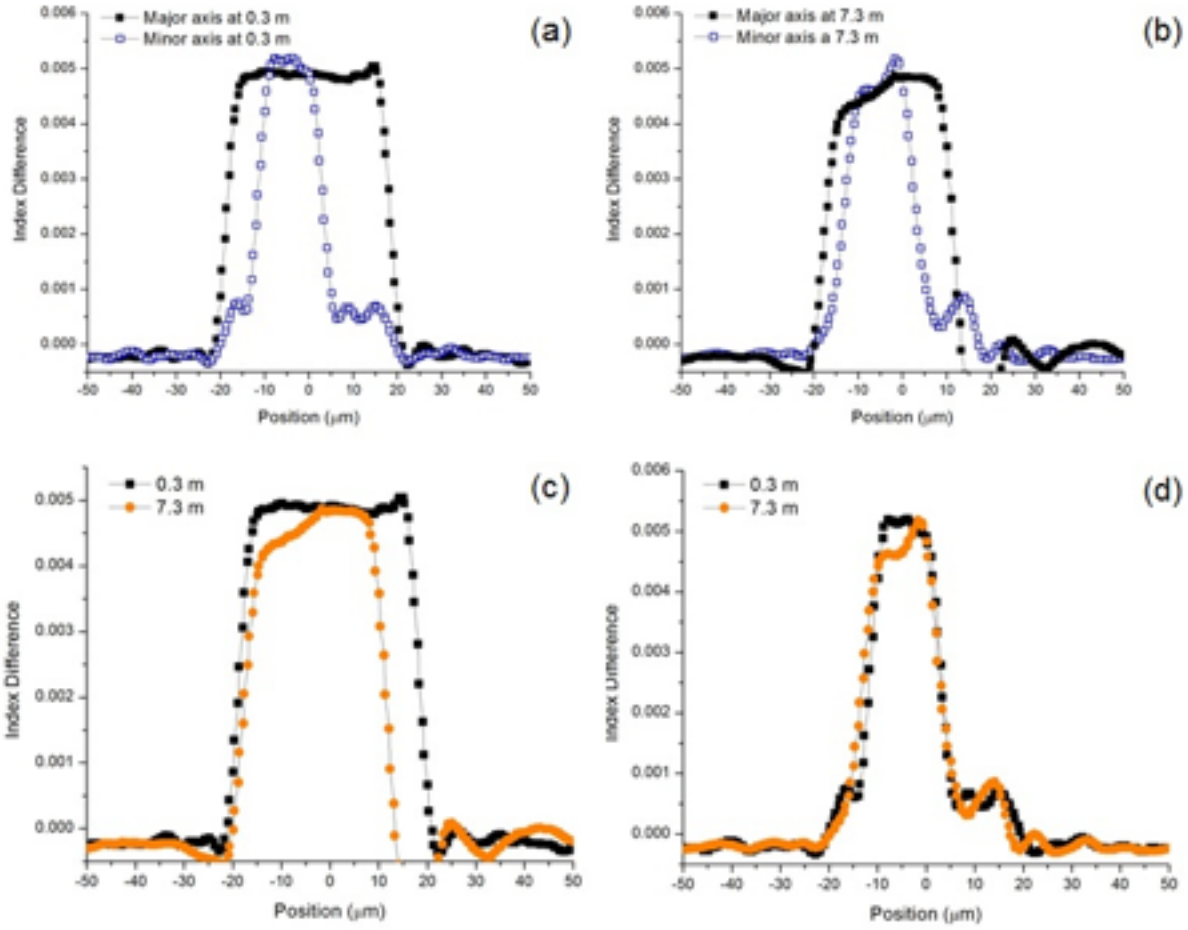

Figure 3.14: Refractive index profiles along major and minor dimensions at selected positions along an arbitrary-chosen 10 meter section of the rectilinear core optical fiber: (a) relative position 0.3 m and (b) 7.3 m. Comparison of the refractive index profiles between the two locations (0.3 m and 7.3 m) of the (c) major axis and (d) minor axis.

Relative position along fiber (m)	***Major axis dimension (μm)***	***Minor axis dimension (μm)***	***Aspect Ratio***
0	11.35	4.63	2.45
15	11.14	4.66	2.39
80	12.54	3.34	3.75
85	12.15	2.87	4.23
90	7.82	1.7	4.60

Table 3.1: Compilation of measured core dimensions along the length of the chirped rectilinear fiber.

same and clearly observed are the classic mirror, mist, and hackle fracture regions from the cleave providing evidence for good strength and a high quality core/clad interface. Also observed is that the core dimensions change while the outer fiber diameter does not. So while the figure 3.14 refractive index profiles verify the LGF nature of these fibers over a short length scale, the figure 3.15 images further validate their overall chirped RCF (and slight LGF) nature. Table 1 compiles the major and minor axes dimensions and computed aspect ratio, which is seen to change from about 2.4 to 4.6; a change of about 190 %. Figure 3.15(d) compares the measured (and normalized) minor axis core sizes (Table 1) with position along the fiber with the $2\cdot(1\text{-}x^2)^{1/2}$ dependence noted above and shown graphically in figure 3.13(e). As is observed, the measured and expected normalized values are in very good agreement.

For completeness, and practical consideration, the attenuation of the rectilinear core fiber was measured and is shown in Figure 3.16. Clearly further improvements are needed to reduce the absorption due to hydroxyl (OH) species at about 1380 nm. At that wavelength, the losses in the rectilinear fiber are essentially equivalent to those in the original LGF. That said the measured losses away from the extrinsic OH band are about 50 dB/km.

Interestingly, this approach yields fibers that possesses a uni-dimensional change

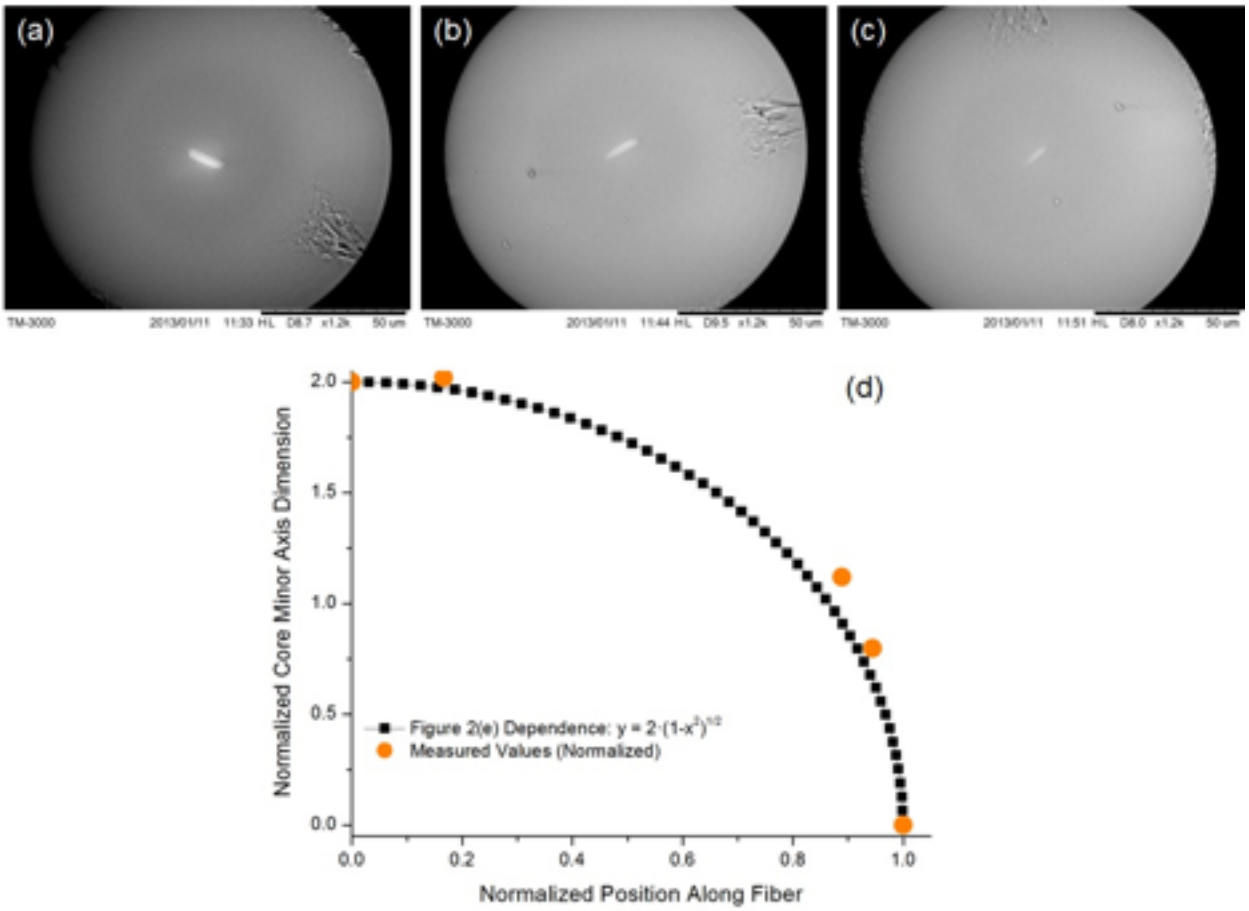

Figure 3.15: (a-c) Scanning electron micrographs of the rectilinear fiber at arbitrary positions along the fibers length. (d) Comparison between measured (and normalized) core size with position along the fiber and the expected dependence described in Figures 2(d) and 2(e).

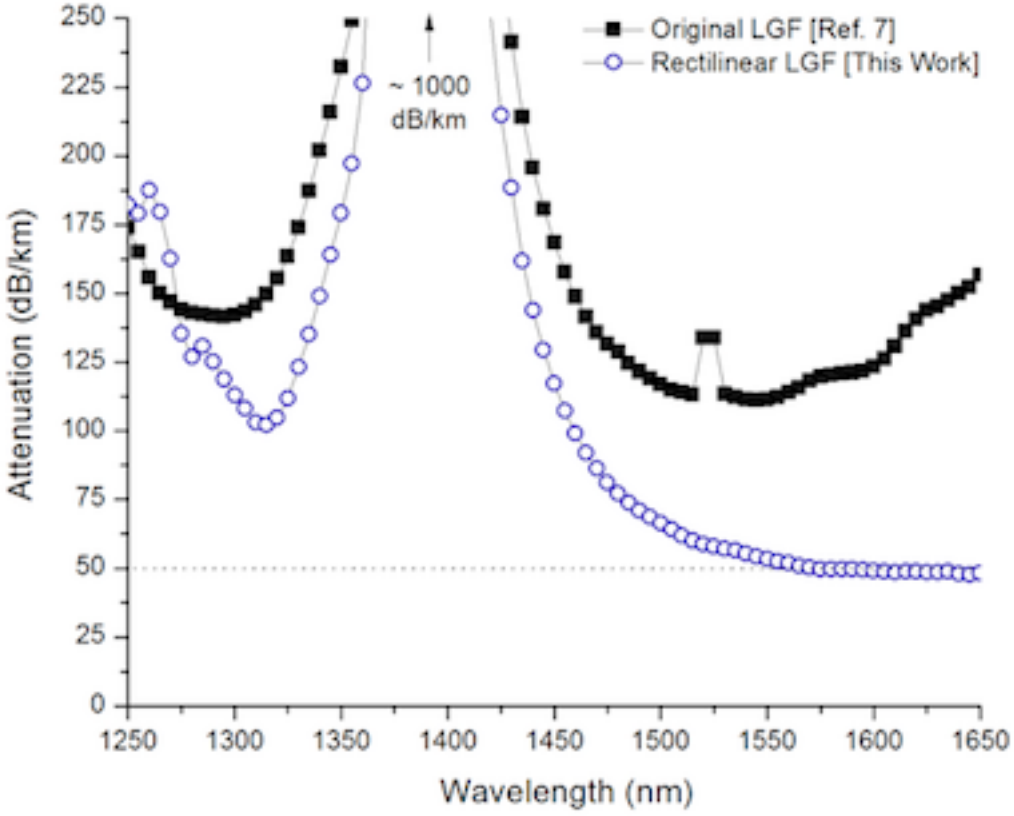

Figure 3.16: Measured attenuation spectrum for a 16 meter length sample of the rectilinear core optical fiber. Also included is the loss spectrum from the original longitudinally-graded optical fiber [3].

in core diameter while all other dimensional attributes remain constant (i.e., the aspect ratio of the rectilinear core changes with length along the fiber). Given the circular cross-section of the initial MCVD-derived core within the side-drilled slug, the variation in the rectilinear core width, w, with distance drawn into the core, x, goes as $2 \cdot (1\text{-}x^2)^{1/2}$.

Chapter 4

Conclusions

4.1 Experimental Conclusions

A new and versatile method for fabricating optical fibers with a longitudinal composition gradient was developed. MCVD-derived germanosilicate fibers were fabricated with a gradient of up to about 0.55 weight % GeO_2 per meter and refractive index difference of about 0.001 over lengths of less than 20 m. The spectral attenuation was 82 dB/km at a wavelength of 1550 nm, which resulted from extrinsic factors and should be diminished with continued optimization. The MCVD-derived germanosilicate LGFs exhibited a Brillouin spectral width broadened by about 3 MHz/m relative to industry standard fibers, though broadening as large as 52 MHz/m is possible with further reduction in fiber attenuation. These gradients enable the possibility of large-scale SBS suppression relative to conventional fibers in fiber lengths <10 m, suitable for fiber laser applications. The measured BGS exhibited a 4.4 dB broadening, relative to a standard single-mode fiber, over a 17 m length of fiber. More generally, these novel LGFs show significant promise for SBS suppression in high energy laser systems as well as a range of other novel applications including constant diameter tapers and

constant grating period chirped Bragg gratings. The process has also been extended to actively doped fiber preforms, ytterbium being the active dopant of choice for the work presented here.

A simple approach to the fabrication of circular outer diameter, silica-based optical fibers possessing rectilinear cores is also shown. The full-width at half-maximum (FWHM) diameter of the larger dimension of the rectangular core was shown to change by 20% over a length of 7 meters. Such rectangular core fibers can be useful for a variety of telecommunication and biomedical applications. Further, the chirp in rectangular dimensions provides for in-situ control of the modal properties of the fiber without resorting to additional external processes such as tapering.

4.2 Theoretical Applications

4.2.1 Potential suppression of four wave mixing

Since the longitudinal refractive index of a fiber core can be controlled by this novel fabrication technique, the efficiency of processes such as four wave mixing (FWM) may be significantly impacted. In high power fiber amplifier arrays where multiple signal frequencies are simultaneously operating, FWM has been observed to yield a parasitic degradation of mutual amplifier coherence. This has been a particularly significant issue for passively phase-locked fiber amplifier arrays [105], which has been partially mitigated by a counter-pumping strategy. The strong longitudinal gradients in refractive index, and expected changes in modal propagation constants, demonstrated in this work can greatly reduce the coherence length for processes like FWM that are strongly impacted by phase-matching of the interacting waves. While a complete analysis of this relatively complex phenomenon has not yet been conducted,

large longitudinal phase-mismatch should be possible for narrowly-spaced optical frequencies in high power amplifiers employing longitudinally-index-graded fibers. The extensive treatments of FWM suppression in telecom fibers can be adapted for modeling high power fiber amplifiers [106].

4.2.2 Constant diameter optical fiber tapers

Optical fibers whose dimensions have been modified by means of a tapering process are useful for modifying or otherwise controlling numerical aperture and dispersion and have been used for supercontinuum generation among other all-fiber devices [107], [108], [109], [110], [111]. Typically, the fiber is heated locally while also being strained such that a region of the fiber is drawn down in size. This dimensional reduction, most notably on core size, influences the numerical aperture and dispersion characteristics of the guided modes. However, while clearly useful, the process inevitably requires great care in order to achieve the desired dimensional reduction, including the shape of the tapered region [112], forces removal of the polymeric coatings that provide mechanical protection to the fiber, and generally lessens the effective strength of the fiber.

The longitudinally-graded optical fibers could serve many of the roles of tapered fibers while maintaining a constant diameter. At a given wavelength the normalized frequency or V-value of the waveguide is defined in terms of the numerical aperture and the core size. In conventional optical fibers, the numerical aperture is independent of position along the fiber length and, as such, the only practical way to control the modal characteristics are to modify the core size; i.e., taper the fiber. In the LGFs, the numerical aperture can be tailored as a function of length along the fiber and, as such, the modal characteristics of the fiber can be influenced without

changing the core size. Interestingly, changes to dispersion are analogous to gain and loss to solitons [113] and so these LGFs might be useful for pulse shaping in the non-linear regime. Of course, one could do both employ a tapered longitudinally-graded optical fiber for added effects.

In the proof-of-concept case treated in the work, the longitudinally-graded optical fiber was shown in figure 3.1 to exhibit an index difference of 0.001, representing a 0.012746 change in numerical aperture, over a distance of 16.6 m. Placed in the context of tapering without tapering this would have the equivalent impact of a reduction in core size by about 10% if a conventional single mode fiber (e.g., SMF-28^{TM}) was tapered in a usual manner. Typically, though, conventional fiber tapers are shorter than 16 m, as noted above, it is reasonable to fabricate longitudinally-graded optical fibers with steeper gradients (i.e., greater index differences over shorter lengths) thereby reducing the requisite fiber length.

4.2.3 Chirped fiber Bragg gratings (without the chirp)

Fiber Bragg gratings (FBGs) are useful in-fiber devices [114] that reflect wavelengths, λ, that meet the Bragg condition of $\lambda = 2 \cdot n \cdot \Lambda$, where Λ is the grating period and n is the effective index of the optical mode. Chirped fiber Bragg gratings (CFBGs), which have been employed for dispersion compensation [115], exhibit grating periods that change along the fiber length, z; i.e., $\Lambda = \Lambda(z)$. The LGFs treated here, where $n = n(z)$, adds an extra degree-of-freedom in designing chirped fiber Bragg gratings. For example, a CFBG can be produced using a LGF where Λ is constant, which generally is a simpler proposition from a manufacturing perspective.

In another example, typical CFBGs are a few tens-of-centimeters long which sets delays to be be between 10-100 ps. With an longitudinal refractive index gradient

and constant Λ, manufacturing CFBGs on the order of meters becomes feasible. This longer fiber length increases the amount of dispersion or delay that can be imparted on a signal to about a nanosecond.

4.2.4 Reduced insertion loss jumpers between dissimilar fibers

Longitudinally-index graded optical fibers could be used to lessen insertion losses between connecting fibers of differing refractive index. Index differences inevitably lead to Fresnel reflections which can lead to reduced transmission as well as ghosting of signals in communication systems. Fresnel reflections at normal incidence can be greatly reduced (possibly negated) through use of a modified quintic refractive index gradient [116], [117]. A preform possessing the requisite radial graded structure could be fabricated using present chemical vapor deposition methods since most state-of-the-art systems are recipe-driven with software that controls gas flow rates to achieve a desired index profile. Said index profile could be converted into a quintic longitudinal index gradient by the generalized process described in this work.

4.2.5 Graded-rare-earth-doped optical fibers

Rare-earth (RE) doped fibers are typically designed to have a constant longitudinal doping profile, though having control over the longitudinal RE doping level can have substantial benefits with respect to pumping efficiency, extraction efficiency and the impact of nonlinear effects such as SBS and FWM. Using the longitudinal gradient technology described herein, longitudinally-graded RE doping can be achieved assuming, as is often the case, that the RE doping of the original preform is radially-graded along with the concentrations of other species in the core. The benefit of gradient doping for the rectilinear case described above has not been analyzed yet,

but improvements in mode selectivity and polarized operation may be feasible.

4.3 Future Work

Future work should primarily focus on methods to improve surface quality of the drilled core slugs in order to reduce attenuation. It is thought that the rough surface (pits and scratches caused by the drill bit) is a primary cause of the relatively high loss in the resulting fiber due to scattering. Polishing the surfaces of the core slugs, either by chemical etching or flame or mechanical polishing, would help to reduce such losses. Difficulties arise though the in the inherent small dimensions of the core slugs, especially with regards to flame and mechanical polishing. Likewise, work should be done to decrease water contamination, and thus hydroxyl absorption. It is believed that water vapor from the oxy-hydrogen torch used in consolidation of the LGF preforms is easily introduced into the glass by via the numerous layers of cladding glass, especially in the second two experiments due to the higher number of cladding glass layers. Reducing the number of cladding layers, reducing the clearance between each layer, and/or increasing the thickness of the glass (especially near the core slugs) could help reduce hydroxyl absorption.

Additionally, investigating methods to more quickly identify the region of interest in a long length of fiber should be explored. The current method of cutting back and analyzing individual sections of fiber one at a time is too time consuming to lend itself to commercial settings. The incorporation of fluorescent nanoparticles into the soot (smiler to the solution doping process for rare earth elements) is one such possible solution to the location problem.

A third area of future work involves tailoring the size of the core to fit specific applications where either longer or shorter index gradients than described in this

thesis are desired. Larger cores can be realized from preforms fabricated via alternate production methods such as vapor axial deposition and outside vapor deposition. These methods tend to allow the formation of larger core areas when compared to MCVD due to the ability to start with a larger seed (core) rod. Core slugs resulting from these processes could be drilled to larger dimensions, resulting in longer lengths of LGFs upon drawing.

Standardizing the core size to correspond to standard single- and multi-mode fiber core fibers should also be completed to ensure compatibility with current fiber systems. This will also allow the LGFs to be characterized with other common testing apparatuses such as optical time delay reflectometry (OTDR), a common tool in both calculating loss in fibers prior to sale and for finding faults (especially breaks) in long lengths of installed fiber. Unlike regular fibers which show a linear decrease in returned signal, LGFs will show a curved return signal due to the varying refractive index and the way by which OTDRs measure signal.

Finally, drilling the cores from angles other than normal to the parent preform should be considered. Given a standard step-index pre from this would result in a fiber with minimal change in refractive index along the length, but significant changes in the shape of the core (figure 4.1). Upon entering the doped region of the core, one would encounter a semi-circular core cross section. As the diameter of the core fully reaches that of the core slug the cross sectional area would transition to fully circular. Finally, as the doped region is exited a semi-circular cross section would again appear but as a *mirror image* of the cross section encountered on the other end. As an extension, if a graded index were the source of the core slugs, a similar change in cross sectional area would result, as well as a longitudinal gradient in refractive index (figure 4.2).

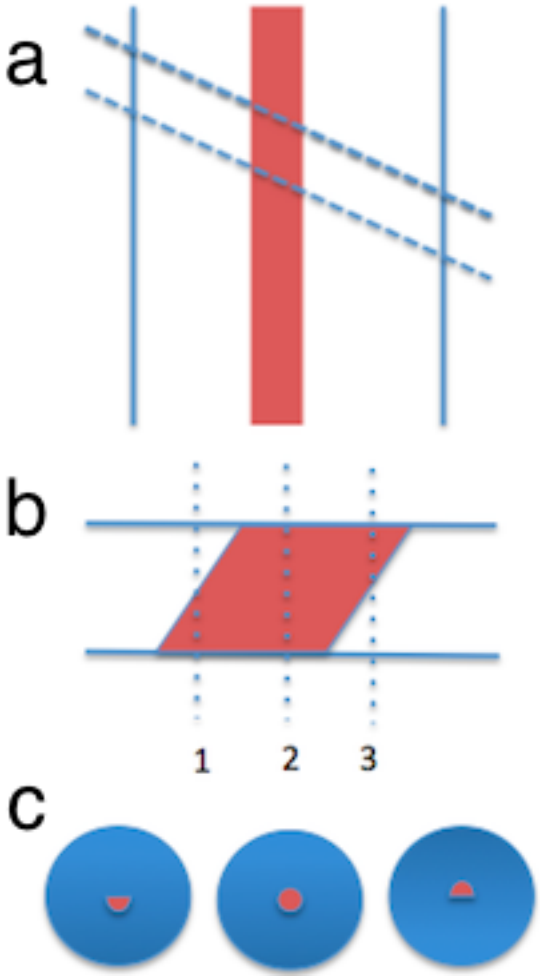

Figure 4.1: Schematic of angled core drilling. The core slugs are drilled from the parent preform at an angle other than normal (a). The resulting fiber (b) will have a generally invariant refractive index profile and longitudinally changing cross sectional area (c). Figure 4.1(c) corresponds with points 1-3 in figure 4.2(b) from left to right.

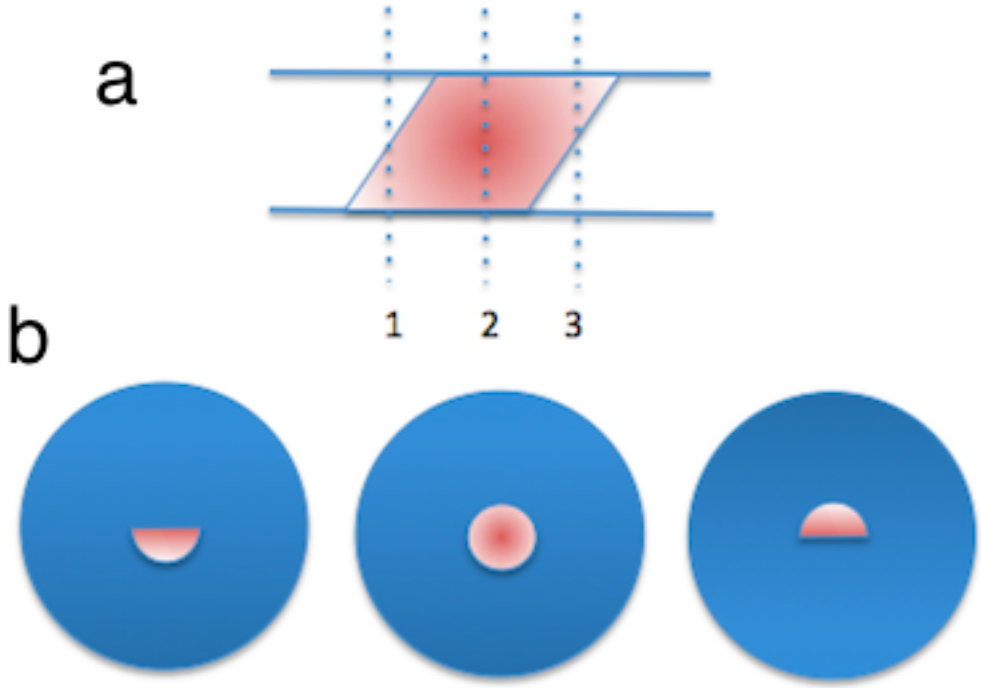

Figure 4.2: Schematic of angled core drilling with graded index parent preform. Figure 4.2(b) corresponds with points 1-3 from left to right.

Appendices

Appendix A Stimulated Brillouin Scattering Mathematical Model, written by Dr. Peter Dragic, UIUC

By way of comparison and potential enhancements with respect to SBS suppression, as is important for high power fiber lasers, the Brillouin gain spectrum (BGS) for a uniform optical fiber is expressed as a Lorentzian function of the frequency ν by

$$g_B(\nu) = g_{B0} \cdot \frac{1}{1 + (\frac{\nu - \nu_0}{\Delta\nu_B/2})^2} \tag{1}$$

where ν_0 is the central frequency and $\Delta\nu_B$ is the Brillouin spectral width (FWHM). The central frequency is determined from a combination of the Bragg condition and the acoustic velocity, V_a, via $\nu_0 = 2n_m V_a/\lambda_0$ with λ_0 being the vacuum optical wavelength and n_m the effective modal index. In equation 1, g_{B0} is the peak Brillouin gain coefficient, which is a function of V_a, $\Delta\nu_B$, n, mass density, and the photoelastic constant [118]. For LGFs, the central frequency becomes a function of distance; i.e., $\nu_0 \rightarrow \nu_0(z)$. For fibers with a lengthwise-uniform refractive index difference, this means that $V_a \rightarrow V_a(z)$ due to the compositional variation. In addition to the acoustic velocity, since $\Delta\nu_B$ is proportional to the square of the central frequency [1], and the central frequency is a function of distance, $\Delta\nu_B$ is also a function of position along the fiber, z. Hence, g_{B0} also is a function of z courtesy of its dependence on V_a and $\Delta\nu_B$.

The ideal configuration, given a maximum end-to-end dopant contrast, is a linear dependence of central frequency with distance along the fiber, z, such that, $\nu_0 \rightarrow \nu_0 - C_z$, where C is a constant. In this case, the Brillouin spectrum is spread uniformly across all available acoustic frequencies, thereby minimizing the Brillouin

gain. In order to compute the measured BGS from such a structure, assume, to first order, that only the central frequency is z-dependent (i.e., the z-dependence of the other parameters is negligible), and that the fiber is optically lossless. Then, with the assumption that equation 1 represents the local BGS in the LGF, integration is performed in order to obtain for the measured BGS that:

$$g_B^{LVF}(\nu) = \frac{\Delta\nu_B}{2LC}(ArcTan[2\frac{(\nu-\nu_0)+CL}{\Delta\nu_B}] - ArcTan[2\frac{(\nu-\nu_0)}{\Delta\nu_B}]) \qquad (2)$$

Next, assume a starting central frequency (i.e., at one end) of 11 GHz and a spectral width of 30 MHz to approximately match the measured characteristics of the SMF-28^{TM} fiber. The fiber length, L, is assumed to be 20 m, which is approximately the length of the LGF with highest gradient. Equation 2 has been normalized so that the total integrated Brillouin gain (with respect to ν) is conserved between uniform and LGFs [95] and that the maximum Brillouin gain in a uniform fiber is unity.

Finally, a value for C must be assumed. For small [Ge] (< 10 weight percent GeO_2), the acoustic velocity is known to decrease by about 0.4% per weight percent of GeO_2 when added to silica [119]. In more recent data than [120], the addition of F to silica was taken to decrease the acoustic velocity by 2.7% per weight percent of F [121]. From these references, the refractive index dependencies on concentration are +0.79x10^{-3} /weight percent and -4.77x10^{-3} /weight percent for GeO_2 and F, respectively. Further, assume that these linear coefficients hold up to 10% GeO_2 and that the fiber is desired to possess a core-cladding index difference of about 5x10-3, which is similar to standard SMF-28^{TM}. At the two fiber ends, the dopant concentrations become [GeO_2, F] = [6.33, 0] and [10.0, 0.61] weight percent (if the maximum GeO_2 content is limited to 10 weight percent), which is quite reasonable to

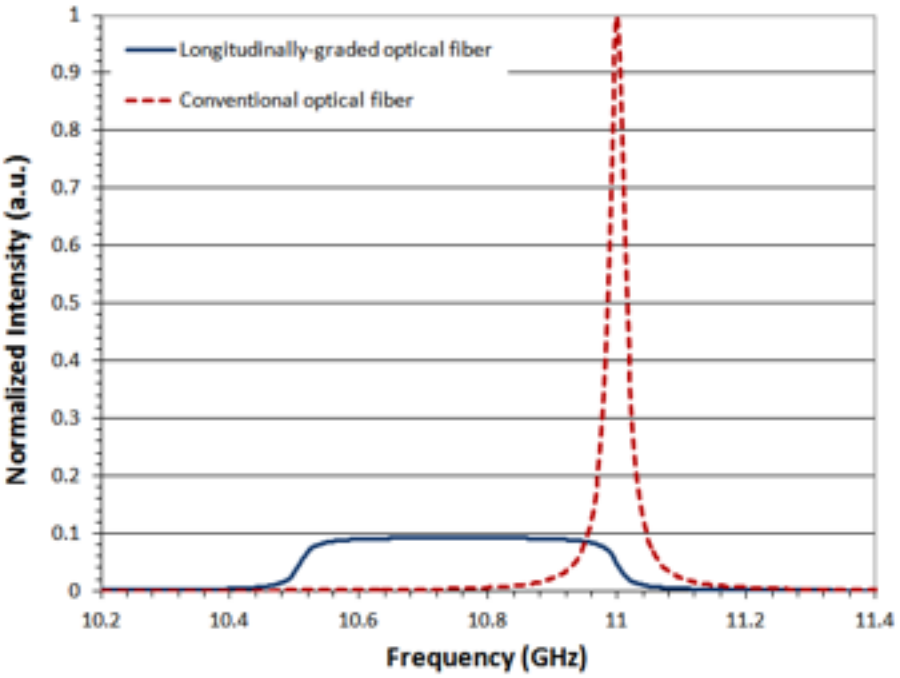

Figure 3: Simulated comparison of the Brillouin gain spectrum (BGS) for a longitudinally-graded optical fiber (solid blue curve) and a conventional longitudinally-uniform (dotted red curve) optical fiber utilizing the coefficients noted in the text. Length-wise dependence of Brillouin spectral width, $\Delta\nu_B$, and peak Brillouin gain coefficient, g_{B0}, has been neglected.

fabricate. This gives rise to acoustic velocities of 5819 m/s and 5558 m/s, respectively, assuming that the acoustic velocity of pure silica is 5970 m/s [119]. Utilizing a modal index of 1.446 and an optical wavelength of 1534 nm, C = 24.6 MHz/m for the assumed L = 20 m.

Figure 3 shows a plot of equation 2, calculated using the coefficients determined above, compared with the simulated BGS of a length-wise uniform fiber with [GeO_2, F] = [6.33, 0] weight percent. The spectrum of the LGF is about 15 times wider than that of the uniform fiber ($\sim$ 500 MHz), and the gain coefficient is decreased by about 10 dB for a very reasonable doping gradient. By comparison, applying a length-wise

thermal gradient to the fiber may also offer similar performance since $\nu_0 \rightarrow \nu_0 + \mathrm{CT}$ where T is the local fiber temperature (*N.B.*, heating the fiber increases the Stokes frequency). A typical value of C for lightly-doped fibers is about 1.2 MHz/K near 1550 nm [29] and is known to decrease with increasing GeO_2 content, thus requiring a 400K thermal gradient to achieve the same broadening as in the LGF example. This thermal gradient is unreasonable for state-of-the-art polymeric buffer coatings and is costly and difficult to implement. Similarly, an applied strain gives rise to $\nu_0 \rightarrow \nu_0 + \mathrm{C}\epsilon$, where ϵ is the elongation of the fiber (in percent, %). C" is approximately 500 MHz/% [29], and thus an applied fiber elongation of 1% is required. Although this is not entirely unreasonable, long-term strain of this magnitude can lead to early fiber failure, and mechanical systems designed to implement such a strain can be complex, bulky, and unstable (drift) over long periods of time.

While the ideal configuration is that of a linear gradient of acoustic frequencies along the fiber length, the distribution in a real fiber may depart somewhat from linear. For example, the gradients identified in figure 2.5 in the main text appear to have a sigmoidal departure from linear, due to dopant diffusion processes during the manufacture of the initial preform. In this case, the slopes of the central frequencies (MHz/m) near the fiber ends are less than that of a simple line connecting the two points. This causes a local enhancement of the Brillouin gain relative to a linearly gradient fiber.

To illustrate this point, we model this diffusion process using the sigmoid function

$$\nu_0(z) = \frac{A}{1 + exp[(B - z)/D]} \tag{3}$$

where A, B, and D are arbitrary constants. Figure 4 shows a plot of the

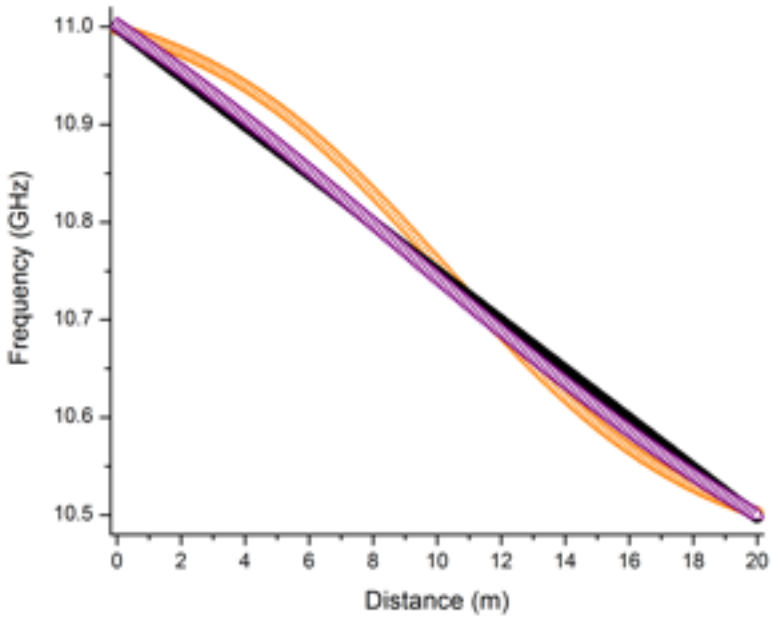

Figure 4: Two sigmoid central frequency gradients (black and blue) plotted with the simple linear gradient of the first example (red).

resulting lengthwise central frequency distributions for two different sets of sigmoid constants, along with a purely linear gradient. Inserting equation 3 into equation 1 and integrating over the fiber length as with the linear case leads to an analytical expression for the Brillouin gain coefficient. Due to the size of this equation, however, it is not provided here.

Rather, plots of the Brillouin spectra corresponding to the distributions of figure 4 are provided in figure 5, It becomes very clear that a strong departure from a linear distribution of central frequencies leads to an enhancement in the Brillouin gain in the spectral regions corresponding to the lower slopes in the spatial dopant distributions. In the case of the example in figure 4, there is a nearly 50% increase in the peak of the Brillouin gain coefficient, with the strongest SBS interaction occurring in the first several meters of fiber. Interestingly, the asymmetry seen in the example

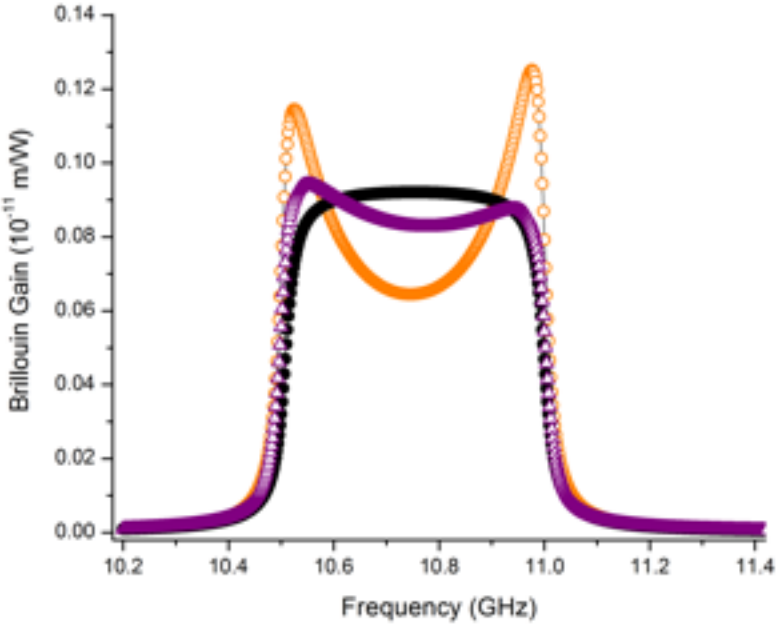

Figure 5: Brillouin gain spectra corresponding to the lengthwise central frequency distributions provided in figure 4.

distributions of figure 4 are clearly manifested as asymmetries in the corresponding Brillouin spectra.

Bibliography

[1] G. Agrawal. *Nonlinear Fiber Optics*. Academic Press, New York, 1995.

[2] Andrey Kobyakov, Michael Sauer, and Dipak Chowdhury. Stimulated brillouin scattering in optical fibers. *Adv. Opt. Photon.*, 2(1):1–59, Mar 2010.

[3] A. Evert, A. James, T. Hawkins, P. Foy, R. Stolen, P. Dragic, L. Dong, R. Rice, and J. Ballato. Longitudinally-graded optical fibers. *Opt. Express*, 20(16):17393–17401, Jul 2012.

[4] D. Keck. A future full of light. *Selected Topics in Quantum Electronics, IEEE Journal of*, 6(6):1254 –1258, nov.-dec. 2000.

[5] Craig Freudenrich. How fiber optics work, March 2001.

[6] F. Hanawa, S. Sudo, M. Kawachi, and M. Nakahara. Fabrication of completely oh-free v.a.d. fibre. *Electronics Letters*, 16(18):699 –700, 28 1980.

[7] W. Vogel. *Chemistry of Glass*. The American Ceramic Society., Westerville, OH, USA, 1985.

[8] Herman Wagter. Fiber-to-the-x: the economics of last-mile fiber, March 2010.

[9] V.A. Bogatyrev, M.M. Bubnov, E.M. Dianov, A.S. Kurkov, P.V. Mamyshev, A.M. Prokhorov, S.D. Rumyantsev, V.A. Semenov, S.L. Semenov, A.A. Sysoliatin, S.V. Chernikov, A.N. Gur'yanov, G.G. Devyatykh, and S.I. Miroshnichenko. A single-mode fiber with chromatic dispersion varying along the length. *Lightwave Technology, Journal of*, 9(5):561 –566, may 1991.

[10] J. Hansryd, F. Dross, M. Westlund, P. A. Andrekson, and S. N. Knudsen. Increase of the sbs threshold in a short highly nonlinear fiber by applying a temperature distribution. *J. Lightwave Technol.*, 19(11):1691, Nov 2001.

[11] N. Yoshizawa, T. Horiguchi, and T. Kurashima. Proposal for stimulated brillouin scattering suppression by fibre cabling. *Electronics Letters*, 27(12):1100 –1101, june 1991.

[12] Ming-Jun Li, Shenping Li, and Daniel A. Nolan. Nonlinear fibers for signal processing using optical kerr effects. *J. Lightwave Technol.*, 23(11):3606, Nov 2005.

[13] J. M. Chavez Boggio, J. D. Marconi, and H. L. Fragnito. Experimental and numerical investigation of the sbs-threshold increase in an optical fiber by applying strain distributions. *J. Lightwave Technol.*, 23(11):3808, Nov 2005.

[14] Kazuhide Nakajima, Masaharu Ohashi, Kazuyuki Shiraki, Tsuneo Horiguchi, and Yoshiaki Miyajima. Four-wave mixing suppression effect of dispersion distributed fibers. *J. Lightwave Technol.*, 17(10):1814, Oct 1999.

[15] R. Stolen. Polarization effects in fiber raman and brillouin lasers. *Quantum Electronics, IEEE Journal of*, 15(10):1157 – 1160, oct 1979.

[16] M. Ohashi and M. Tateda. Design of strain-free-fiber with nonuniform dopant concentration for stimulated brillouin scattering suppression. *Lightwave Technology, Journal of*, 11(12):1941 –1945, dec 1993.

[17] K. Shiraki, M. Ohashi, and M. Tateda. Performance of strain-free stimulated brillouin scattering suppression fiber. *Lightwave Technology, Journal of*, 14(4):549 –554, apr 1996.

[18] L. M. Pedrotti F. Pedrotti, L.S. Pedrotti. *Introduction to Optics, Third Edition*. Pearson Education, Inc., San Francisco, CA, USA, 2007.

[19] Mark Fox. *Optical Properties of Solids*. Oxford University Press, Oxford, England, 2010.

[20] Chai Yeh. *Applied Photonics*. Academic Press, Inc., San Diego, CA, USA, 1994.

[21] Alan Willner Leonid Kazovsky, Sergio Benedetto. *Optical Fiber Communication Systems*. Artech House, Norwood, MA, USA, 1996.

[22] D.Y. Tang, P.D. Drummond, W.S. Man, H.Y. Tam, and M.S. Demokan. Observation of modulation instability in a fibre soliton laser. In *Lasers and Electro-Optics, 1999. CLEO/Pacific Rim '99. The Pacific Rim Conference on*, volume 2, pages 417 –418 vol.2, 1999.

[23] Roger L. Freeman. *Fiber-Optic Systems for Telecommunications*. John Wiley Sons, Inc., New York, NY, USA, 2002.

[24] R. Stolen and J. Bjorkholm. Parametric amplification and frequency conversion in optical fibers. *Quantum Electronics, IEEE Journal of*, 18(7):1062 – 1072, jul 1982.

[25] S. Wen. Optical phase conjugation of multiwavelength signals in a dispersion-shifted fiber. *Lightwave Technology, Journal of*, 15(7):1061 –1070, jul 1997.

[26] M. Sauer, D. Nolan, M. Li, and G. Berkey. Simultaneous multichannel pulse compression for broadband dynamic dispersion compensation. In *Optical Fiber Communications Conference, 2003. OFC 2003*, pages 298 – 300 vol.1, march 2003.

[27] L. Brillouin. Diffusion de la luminere par un corps transparent homogene. *Ann. Phys.*, 17(88), 1922.

[28] R. Y. Chiao, C. H. Townes, and B. P. Stoicheff. Stimulated brillouin scattering and coherent generation of intense hypersonic waves. *Phys. Rev. Lett.*, 12:592–595, May 1964.

[29] M. Nikles, L. Thevenaz, and P.A. Robert. Brillouin gain spectrum characterization in single-mode optical fibers. *Lightwave Technology, Journal of*, 15(10):1842 –1851, oct 1997.

[30] V. Sundar and R.E. Newnham. *The Electrical Engineering Handbook, 2nd edition.* CRC Press., Boca Raton, FL, USA, 1997.

[31] A.B. Ruffin. Stimulated brillouin scattering: an overview of measurements, system impairments, and applications. In *Optical Fiber Measurements, 2004. Technical Digest: Symposium on*, pages 23 – 28, 2004.

[32] R.W. Boyd, K. Rzazewski, and P. Narum. Noise initiation of stimulated brillouin scattering. *Phys. Rev. A, At. Mol. Opt. Phys. (USA)*, 42(9):5514 – 21, 1990/11/01.

[33] A. Yeniay, J.-M. Delavaux, and J. Toulouse. Spontaneous and stimulated brillouin scattering gain spectra in optical fibers. *Lightwave Technology, Journal of*, 20(8):1425 – 1432, aug 2002.

[34] K. Shiraki, M. Ohashi, and M. Tateda. Suppression of stimulated brillouin scattering in a fibre by changing the core radius. *Electronics Letters*, 31(8):668 –669, apr 1995.

[35] N. Yoshizawa and T. Imai. Stimulated brillouin scattering suppression by means of applying strain distribution to fiber with cabling. *Lightwave Technology, Journal of*, 11(10):1518 –1522, oct 1993.

[36] R. G. Smith. Optical power handling capacity of low loss optical fibers as determined by stimulated raman and brillouin scattering. *Appl. Opt.*, 11(11):2489–2494, Nov 1972.

[37] Y. Aoki, K. Tajima, and I. Mito. Input power limits of single-mode optical fibers due to stimulated brillouin scattering in optical communication systems. *Lightwave Technology, Journal of*, 6(5):710 –719, may 1988.

[38] X.S. Yao. Brillouin selective sideband amplification of microwave photonic signals. *Photonics Technology Letters, IEEE*, 10(1):138 –140, jan. 1998.

[39] Takuo Tanemura, Yuichi Takushima, and Kazuro Kikuchi. Narrowband optical filter, with a variable transmission spectrum, using stimulated brillouin scattering in optical fiber. *Opt. Lett.*, 27(17):1552–1554, Sep 2002.

[40] Andreas Wiberg and Per Olof Hedekvist. Photonic microwave generator utilizing narrowband brillouin amplification and a fiber-based oscillator. pages 148–156, 2004.

[41] Liang Xing, Li Zhan, Shouyu Luo, and Yuxing Xia. High-power low-noise fiber brillouin amplifier for tunable slow-light delay buffer. *Quantum Electronics, IEEE Journal of*, 44(12):1133 –1138, dec. 2008.

[42] A.D. Ellis, Jian Zhao, and D. Cotter. Approaching the non-linear shannon limit. *Lightwave Technology, Journal of*, 28(4):423 –433, feb.15, 2010.

[43] Johan Nilsson. High power fiber lasers. In *Lasers and Electro-Optics (CLEO) and Quantum Electronics and Laser Science Conference (QELS), 2010 Conference on*, pages 1 –2, may 2010.

[44] D. J. Richardson, J. Nilsson, and W. A. Clarkson. High power fiber lasers: current status and future perspectives. *J. Opt. Soc. Am. B*, 27(11):B63–B92, Nov 2010.

[45] Jr. Cerqueira, S.A. Recent progress and novel applications of photonic crystal fibers. *Rep. Prog. Phys. (UK)*, 73(2):024401 (21 pp.) –, 2010/02/.

[46] Johan Nilsson. Recent progress and limiting factors in high power fiber laser technology. In *Conference on Lasers and Electro-Optics*, page CTuC1. Optical Society of America, 2010.

[47] Robert R. Rice, Michael G. Wickham, Hiroshi Komine, Peter Livingston, Peter Thielen, and Charles Phillip Asman. Optical fiber amplifier and methods of making the same, Sept 2010.

[48] V.V. Cherny. Confined guided modes in w-fibre with square core. *Electronics Letters*, 15(10):281 –282, 10 1979.

[49] F. Ladouceur, J.D. Love, and I.M. Skinner. Single mode square- and rectangular-core waveguides. *Optoelectronics, IEE Proceedings J*, 138(4):253 –260, aug 1991.

[50] V. Ramaswamy, W. G. French, and R. D. Standley. Polarization characteristics of noncircular core single-mode fibers. *Appl. Opt.*, 17(18):3014–3017, Sep 1978.

[51] V. V. Cherny, G. A. Juravlev, A. I. Kirpa, and V. R. Tjoy. Multi-mode and single-mode optical fiber guides with rectangular core for communication systems. pages 173–177, 1979.

[52] Amber L. Bullington, Paul H. Pax, Arun K. Sridharan, John E. Heebner, Michael J. Messerly, and Jay W. Dawson. Mode conversion in rectangular-core optical fibers. *Appl. Opt.*, 51(1):84–88, Jan 2012.

[53] Todd E. Lizotte. Laser beam uniformity and stability using homogenizer-based fiber optic launch method: square core fiber delivery. pages 78940Y–78940Y–10, 2011.

[54] David A. Rockwell, Vladimir V. Shkunov, and John R. Marciante. Semi-guiding high-aspect-ratio core (sharc) fiber providing single-mode operation and an ultra-large core area in a compact coilable package. *Opt. Express*, 19(15):14746–14762, Jul 2011.

[55] M. Braglia, G. Cocito, G. Grego, E. Modone, and G. Parisi. Noncircular core optical fibres made by pressurized mcvd method. *CSELT Technical Reports*, 14(6):423 – 425, 1986.

[56] Eros Modone Giuseppe Cocito, Giorgio Grego. Method of producing optical fibers with noncircular cores, Apr 1988.

[57] At present, non-circular fibers are available commercially from nlight (liekki); see: http://www.nlight.net.

[58] Amber L. Bullington, Paul H. Pax, Arun K. Sridharan, John E. Heebner, Michael J. Messerly, and Jay W. Dawson. Mode conversion in rectangular-core optical fibers. *Appl. Opt.*, 51(1):84–88, Jan 2012.

[59] K.D. Dambul, N. Tamchek, S.R. Sandoghchi, M.R. Abu Hassan, D.C. Tee, and F.R. Mahamd Adikan. Fabrication and characterization of flat fibers. In *Photonics (ICP), 2011 IEEE 2nd International Conference on*, pages 1–4, oct. 2011.

[60] J.R. Haynes, J.C. Baggett, T.M. Monro, D.J. Richardson, P. Grunewald, and R. Allott. Square core jacketed air-clad fiber. In *Optical Fiber Communication Conference, 2006 and the 2006 National Fiber Optic Engineers Conference. OFC 2006*, page 3 pp., march 2006.

[61] Gilhwan Kim, Taiyong Cho, Kyujin Hwang, Kwanil Lee, Kyung Shik Lee, and Sang Bae Lee. Experimental characterization of elliptical hollow-core photonic bandgap fiber at wavelengths within the bandgap. In *Optical Fiber Communication - incudes post deadline papers, 2009. OFC 2009. Conference on*, pages 1 –3, march 2009.

[62] Wenrui Xue, Ya nan Guo, Peng Li, and Wenmei Zhang. Propagation properties of a surface plasmonic waveguide with double elliptical air cores. *Opt. Express*, 16(14):10710–10720, Jul 2008.

[63] V. Ramaswamy, W. G. French, and R. D. Standley. Polarization characteristics of noncircular core single-mode fibers. *Appl. Opt.*, 17(18):3014–3017, Sep 1978.

[64] Douglas J. Markos, Benjamin L. Ipson, Kevin H. Smith, Stephen M. Schultz, Richard H. Selfridge, Thomas D. Monte, Richard B. Dyott, and Gregory Miller. Controlled core removal from a d-shaped optical fiber. *Appl. Opt.*, 42(36):7121–7125, Dec 2003.

[65] Stephanie Morris, Colin McMillen, Thomas Hawkins, Paul Foy, Roger Stolen, John Ballato, and Robert Rice. The influence of core geometry on the crystallography of silicon optical fiber. *Journal of Crystal Growth*, 352(1):53 – 58, 2012.

[66] Thomas Rasmussen, Jørn Hedegaard Povlsen, and Anders Bjarklev. Optimization of beam propagation methods for waveguide structures with rectangular core cross sections. In *Integrated Photonics Research*, page ThB2. Optical Society of America, 1994.

[67] K. Konishi, T. Kanie, K. Takahashi, O. Shimakawa, Y. Mitose, T. Sasaki, T. Taru, T. Nagashima, K. Fuse, and A. Inoue. Development of rectangular core optical fiber cable for high power laser. *SEI Tech. Rev. (Japan)*, (71):109 – 12, 2010/10/.

[68] B. Malinsky, T. Monte, T. Kubo, J. Brunner, and Wenxin Zheng. Automatic alignment and splicing for elliptical core d-fiber. In *Optical Fiber Communication - incudes post deadline papers, 2009. OFC 2009. Conference on*, pages 1 –3, march 2009.

[69] S. T. Huntington, K. A. Nugent, A. Roberts, P. Mulvaney, and K. M. Lo. Field characterization of a d-shaped optical fiber using scanning near-field optical microscopy. *Journal of Applied Physics*, 82(2):510 –513, jul 1997.

[70] F.A. Muhammad and G. Stewart. D-shaped optical fibre design for methane gas sensing. *Electronics Letters*, 28(13):1205 –1206, june 1992.

[71] Waclaw Urbanczyk, Tadeusz Martynkien, and Wojtek J. Bock. Dispersion effects in elliptical-core highly birefringent fibers. *Appl. Opt.*, 40(12):1911–1920, Apr 2001.

[72] S. Nagel, J. MacChesney, and K. Walker. An overview of the modified chemical vapor deposition (mcvd) process and performance. *Quantum Electronics, IEEE Journal of*, 18(4):459 –476, april 1982.

[73] A.D. Yablon. Multi-wavelength optical fiber refractive index profiling by spatially resolved fourier transform spectroscopy. *Lightwave Technology, Journal of*, 28(4):360 –364, feb.15, 2010.

[74] Andrew Yablon. personal communication, January 2012.

[75] R.W. Tkach, A.R. Chraplyvy, and R.M. Derosier. Spontaneous brillouin scattering for single-mode optical-fibre characterisation. *Electronics Letters*, 22(19):1011 –1013, 11 1986.

[76] P.D. Dragic. Estimating the effect of ge doping on the acoustic damping coefficient via a highly ge-doped mcvd silica fiber. *J. Opt. Soc. Am. B, Opt. Phys. (USA)*, 26(8):1614 – 20, 2009/08/.

[77] Y.H. Kim, U.-C. Paek, and W.-T. Han. Fiber length dependence of phase change induced by laser-diode pumping in yb/sup 3+/-al/sup 3+/ co-doped optical fibers. *Photonics Technology Letters, IEEE*, 14(12):1710 –1712, dec. 2002.

[78] P.C. Becker, N.A. Olson, and J.R. Simpson. *Erbium Doped Fiber Amplifiers-Fundamentals and Technology*. Academic., New York, NY, USA, 1999.

[79] S.B. Poole, D.N. Payne, and M.E. Fermann. Fabrication of low-loss optical fibres containing rare-earth ions. *Electronics Letters*, 21(17):737 –738, 15 1985.

[80] J.E. Townsend, S.B. Poole, and D.N. Payne. Solution-doping technique for fabrication of rare-earth-doped optical fibres. *Electronics Letters*, 23(7):329 – 331, 26 1987.

[81] Ranjan Sen, Mrinmay Pal, Mukul Chandra Paul, Shyamal Kumar Bhadra, Somesh Chatterjee, and Kamal Dasgupta. Method of fabricating rare earth doped optical fibre, Feb 2005.

[82] Martin Leich, Florian Just, Andreas Langner, Mario Such, Gerhard Schötz, Tina Eschrich, and Stephan Grimm. Highly efficient yb-doped silica fibers prepared by powder sinter technology. *Opt. Lett.*, 36(9):1557–1559, May 2011.

[83] S.K. Bhadra, R. Sen, M. Pal, M.C. Paul, M.K. Naskar, S. Chatterjee, M. Chatterjee, and K. Dasgupta. Development of rare-earth doped fibres for amplifiers in wdm systems. *Circuits, Devices and Systems, IEE Proceedings* -, 150(6):480 – 485, dec. 2003.

[84] R.J. Mears, L. Reekie, I.M. Jauncey, and D.N. Payne. Low-noise erbium-doped fibre amplifier operating at 1.54 x003bc;m. *Electronics Letters*, 23(19):1026 –1028, 10 1987.

[85] Yasutake Ohishi, Terutoshi Kanamori, Takeshi Kitagawa, Shiro Takahashi, Elias Snitzer, and Jr. George H. Sigel. Pr3+-doped fluoride fiber amplifier operating at 1.31 m. *Opt. Lett.*, 16(22):1747–1749, Nov 1991.

[86] E. Snitzer. Proposed fiber cavities for optical masers. *Journal of Applied Physics*, 32(1):36 –39, jan 1961.

[87] Frederik Nielsen, Lars Thrane, John Black, Anders Bjarklev, and Peter Andersen. Swept wavelength source in the 1 m range. *Opt. Express*, 13(11):4096–4106, May 2005.

[88] R. Paschotta, J. Nilsson, A.C. Tropper, and D.C. Hanna. Ytterbium-doped fiber amplifiers. *Quantum Electronics, IEEE Journal of*, 33(7):1049 –1056, jul 1997.

[89] B.J. Ainslie. A review of the fabrication and properties of erbium-doped fibers for optical amplifiers. *Lightwave Technology, Journal of*, 9(2):220 –227, feb 1991.

[90] D.C. Hanna, R.M. Percival, I.R. Perry, R.G. Smart, P.J.M. Suni, J.E. Townsend, and A.C. Tropper. Continuous-wave oscillation of a monomode ytterbium-doped fibre laser. In *All-Fibre Devices, IEE Colloquium on*, pages 14/1 –14/4, jun 1988.

[91] Chi Liu, Yunfeng Qi, Yaqian Ding, Jun Zhou, Jingxing Dong, Yunrong Wei, and Qihong Lou. All-fiber, high power single-frequency linearly polarized ytterbium-doped fiber amplifier. *Chin. Opt. Lett.*, 9(3):031402, Mar 2011.

[92] Wang Jing, Li Jian, Liu Peng, Mao XiangQiao, Wang Lin, Liu LiSong, Peng Jian, Zhang ChenFang, Zheng Kai, Wei Huai, Fu Yong Jun, Yan FengPing, Ning TiGang, and Jian Wei. Fabrication and characteristics of yb3+-doped silica optical fibers. In *Optical Fiber Communication Optoelectronic Exposition Conference, 2008. AOE 2008. Asia*, pages 1 –3, 30 2008-nov. 2 2008.

[93] P. Barua, E.H. Sekiya, K. Saito, and A.J. Ikushima. Influences of yb3+ ion concentration on the spectroscopic properties of silica glass. *J. Non-Cryst. Solids (Netherlands)*, 354(42-44):4760 – 4, 2008/11/01.

[94] Jun Dong, Michael Bass, Yanli Mao, Peizhen Deng, and Fuxi Gan. Dependence of the yb3+ emission cross section and lifetime on temperature and concentration in yttrium aluminum garnet. *J. Opt. Soc. Am. B*, 20(9):1975–1979, Sep 2003.

[95] Benjamin Ward and Justin Spring. Finite element analysis of brillouin gain in sbs-suppressing optical fibers with non-uniform acoustic velocity profiles. *Opt. Express*, 17(18):15685–15699, Aug 2009.

[96] Evgeny M. Dianov and Valery M. Mashinsky. Germania-based core optical fibers. *J. Lightwave Technol.*, 23(11):3500, Nov 2005.

[97] Kyunghwan Oh and Un-Chul Paek. *Silica Optical Fiber Technology for Device and Components: Design, Fabrication, and International Standards*. John Wiley Sons, Inc., New York, NY, USA, 2012.

[98] E.J. Bochove and S.A. Shakir. Analysis of a spatial-filtering passive fiber laser beam combining system. *Selected Topics in Quantum Electronics, IEEE Journal of*, 15(2):320 –327, march-april 2009.

[99] D. Marcuse and R.M. Derosier. Mode conversion caused by diameter changes of a round dielectric waveguide. *Bell Syst. Tech. J. (USA)*, 48(10):3217 – 32, 1969/12/.

[100] G.E. Town and J.T. Lizier. Tapered holey fibers for spot size and numerical aperture conversion. In *Lasers and Electro-Optics, 2001. CLEO '01. Technical Digest. Summaries of papers presented at the Conference on*, page 261, 2001.

[101] T. A. Birks, W. J. Wadsworth, and P. St. J. Russell. Supercontinuum generation in tapered fibers. *Opt. Lett.*, 25(19):1415–1417, Oct 2000.

[102] N. G. R. Broderick. Method for pulse transformations using dispersion varying optical fibre tapers. *Opt. Express*, 18(23):24060–24069, Nov 2010.

[103] C.R. Giles. Lightwave applications of fiber bragg gratings. *J. Lightwave Technol. (USA)*, 15(8):1391 – 404, 1997/08/.

[104] K.O. Hill, F. Bilodeau, B. Malo, T. Kitagawa, S. Theriault, D.C. Johnson, J. Albert, and K. Takiguchi. Chirped in-fiber bragg gratings for compensation of optical-fiber dispersion. *Opt. Lett. (USA)*, 19(17):1314 – 16, 1 Sept. 1994.

[105] E.J. Bochove and S.A. Shakir. Analysis of a spatial-filtering passive fiber laser beam combining system. *Selected Topics in Quantum Electronics, IEEE Journal of*, 15(2):320 –327, march-april 2009.

[106] K. Nakajima, M. Ohashi, K. Shiraki, T. Horiguchi, K. Kurokawa, and Y. Miyajima. Four-wave mixing suppression effect of dispersion distributed fibers. *Lightwave Technology, Journal of*, 17(10):1814 –1822, oct 1999.

[107] D. Marcuse and R. Derosier. Mode conversion caused by diameter changes of a round dielectric waveguide. *Bell Syst. Tech. J.*, 48(10):3217–3232, Dec 1969.

[108] G.E. Town and J.T. Lizier. Tapered holey fibers for spot size and numerical aperture conversion. In *Lasers and Electro-Optics, 2001. CLEO '01. Technical Digest. Summaries of papers presented at the Conference on*, page 261, 2001.

[109] Kuei-Chu Hsu, Nan-Kuang Chen, Sen-Yih Chou, Shien-Kuei Liaw, Yinchieh Lai, and Sien Chi. Bandwidth-variable bandpass filter based on dispersion engineered tapered fiber with external polymer cladding. In *Optical Fiber Communication - incudes post deadline papers, 2009. OFC 2009. Conference on*, pages 1 –3, march 2009.

[110] T. A. Birks, W. J. Wadsworth, and P. St. J. Russell. Supercontinuum generation in tapered fibers. *Opt. Lett.*, 25(19):1415–1417, Oct 2000.

[111] Tim Birks, George Kakarantzas, and Philip Russell. All-fibre devices based on tapered fibres. In *Optical Fiber Communication Conference*, page ThK2. Optical Society of America, 2004.

[112] T.A. Birks and Y.W. Li. The shape of fiber tapers. *Lightwave Technology, Journal of*, 10(4):432 –438, apr 1992.

[113] N. G. R. Broderick. Method for pulse transformations using dispersion varying optical fibre tapers. *Opt. Express*, 18(23):24060–24069, Nov 2010.

[114] C.R. Giles. Lightwave applications of fiber bragg gratings. *Lightwave Technology, Journal of*, 15(8):1391 –1404, aug 1997.

[115] K. O. Hill, F. Bilodeau, B. Malo, T. Kitagawa, S. Thériault, D. C. Johnson, J. Albert, and K. Takiguchi. Chirped in-fiber bragg gratings for compensation of optical-fiber dispersion. *Opt. Lett.*, 19(17):1314–1316, Sep 1994.

[116] W. H. Southwell. Gradient-index antireflection coatings. *Opt. Lett.*, 8(11):584–586, Nov 1983.

[117] Daniel Poitras and J. A. Dobrowolski. Toward perfect antireflection coatings. 2. theory. *Appl. Opt.*, 43(6):1286–1295, Feb 2004.

[118] P.D. Dragic. Simplified model for effect of ge doping on silica fibre acoustic properties. *Electronics Letters*, 45(5):256 –257, 26 2009.

[119] Peter D. Dragic. The acoustic velocity of ge-doped silica fibers: A comparison of two models. *International Journal of Applied Glass Science*, 1(3):330–337, 2010.

[120] Cheng-Kuei Jen, Christian Neron, Alan Shang, Koich Abe, Lee Bonnell, and Junichi Kushibiki. Acoustic characterization of silica glasses. *Journal of the American Ceramic Society*, 76(3):712 – 716, 1993.

[121] Weiwen Zou, Zuyuan He, and Kazuo Hotate. Experimental study of brillouin scattering in fluorine-doped single-mode optical fibers. *Opt. Express*, 16(23):18804–18812, Nov 2008.